

Convexified Message-Passing Graph Neural Networks

Saar Cohen, Noa Agmon and Uri Shaham

Department of Computer Science

Bar Ilan University, Israel

saar30@gmail.com, agmon@cs.biu.ac.il, uri.shaham@biu.ac.il

Abstract

Graph Neural Networks (GNNs) have become prominent methods for graph representation learning, demonstrating strong empirical results on diverse graph prediction tasks. In this paper, we introduce ***Convexified Message-Passing Graph Neural Networks*** (CGNNs), a novel and general framework that combines the power of message-passing GNNs with the tractability of *convex* optimization. By mapping their nonlinear filters into a reproducing kernel Hilbert space, CGNNs transform training into a convex optimization problem, which can be solved efficiently and optimally by projected gradient methods. This convexity further allows the statistical properties of CGNNs to be analyzed accurately and rigorously. For two-layer CGNNs, we establish rigorous generalization guarantees, showing convergence to the performance of the optimal GNN. To scale to deeper architectures, we adopt a principled layer-wise training strategy. Experiments on benchmark datasets show that CGNNs significantly exceed the performance of leading GNN models, achieving 10–40% higher accuracy in most cases, underscoring their promise as a powerful and principled method with strong theoretical foundations. In rare cases where improvements are not quantitatively substantial, the convex models either slightly exceed or match the baselines, stressing their robustness and wide applicability. Though over-parameterization is often employed to enhance performance in non-convex models, we show that our CGNNs framework yields shallow convex models that can surpass these models in both accuracy and resource efficiency.

1 Introduction

Graphs serve as versatile models across various domains, such as social networks [47], protein design [22], and medical diagnosis [27]. Graph representation learning has thus attracted widespread attention in recent years, with Graph Neural Networks (GNNs) emerging as powerful tools. Message Passing Neural Networks (MPNNs) [18, 20, 45], a most widely adopted class of GNNs, provide a scalable and elegant architecture that effectively exploits a message-passing mechanism to extract useful information and learn high-quality representations from graph data.

In this paper, we present the new and general framework of ***Convexified Message-Passing Graph Neural Networks*** (CGNNs), reducing the training of message-passing GNNs to a *convex* optimization problem solvable efficiently and optimally via projected gradient methods. The convexity of CGNNs offers a distinct advantage: it ensures *global* optimality and computational tractability without relying on, e.g., over-parameterization, unlike many existing approaches [1, 10, 11, 60]. This convexity also enables a precise and theoretically grounded analysis of generalization and statistical behavior.

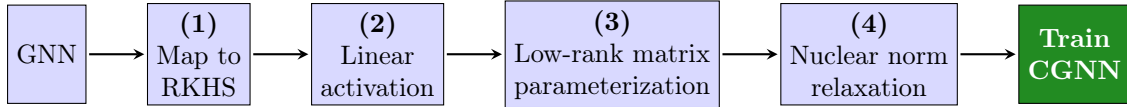


Figure 1: Convexification Procedure of a message-passing GNN into a CGNN.

We exhibit our framework by convexifying two-layer Graph Convolution Networks (GCNs) [7, 24], a widely-used GNN model for learning over graph-structured data. Inspired by the convexification of convolutional neural networks by Zhang et al. [59], we adapt their methodology to the graph domain. A high-level overview of our convexification pipeline is summarized in Figure 1, explained as follows. The key challenge lies in handling GCNs’ nonlinearity: we address this by first relaxing the space of GCN filters to a reproducing kernel Hilbert space (RKHS) (step (1) in Figure 1), effectively reducing the model to one with a linear activation function (step (2)). We then show that GCNs with RKHS filters admit a low-rank matrix representation (step (3)). Finally, by relaxing the non-convex rank constraint into a convex nuclear norm constraint (step (4)), we arrive at our CGCN formulation.

Theoretically, we establish an upper bound on the expected generalization error of our class of two-layer CGCNs, composed of the best possible performance attainable by a two-layer GCN with infinite data and a complexity term that decays to zero polynomially with the number of training samples. Our result dictates that the generalization error of a CGCN provably converges to that of an optimal GCN, offering both strong statistical guarantees and practical relevance. Moreover, our analysis naturally extends to deeper models by applying the argument layer-wise, providing insights into the statistical behavior of multi-layer CGCNs as well.

Finally, we perform an extensive empirical analysis over various benchmark datasets, where our framework exhibits outstanding results. First, we apply our framework to a wide range of leading message-passing GNN models, including GAT [45], GATv2 [4], GIN [51], GraphSAGE [20], and ResGatedGCN [3]. We also extended our framework to hybrid transformer models, specifically GraphGPS [36] and GraphTrans [40, 49], which integrate local message passing GNNs with global attention mechanisms. Remarkably, in most cases, the convex variants outperform the original non-convex counterparts by a large magnitude, obtaining 10–40% higher accuracy, highlighting the practical power of our approach alongside its theoretical appeal. Even in the minority of cases where improvements are modest, the convexified models still match or slightly exceed the baseline performance, further validating the robustness and broad applicability of our method. While over-parameterization is commonly used to boost performance in non-convex models [1, 10, 11, 60], we show that our CGNNs framework enables the construction of shallow convex architectures that outperform over-parameterized non-convex ones in both accuracy and resource efficiency.

2 Related Work

Message-Passing GNNs. Early developments of message-passing GNNs include GCN [7, 24], GAT [45], GIN [51], GraphSAGE [20], and others. Such methods effectively leverage a message-passing mechanism to recursively aggregate useful neighbor information [18], enabling them to learn high-quality representations from graph data. Those models have proven effective across diverse tasks, obtaining state-of-the-art performance in various graph prediction tasks (see, e.g., [5, 20, 36, 45, 51, 55]). Our framework of CGNNs harnesses the power of message-passing GNNs

by transforming training into a *convex* optimization problem. This shift not only enables efficient computation of globally optimal solutions, but also allows an accurate and rigorous analysis of statistical properties.

Convergence of Gradient Methods to Global Optima. A vast line of research analyzed the convergence of gradient-based methods to global optima when training neural networks, but under restrictive conditions. Several works rely on over-parameterization, often requiring network widths far exceeding the number of training samples [1, 11, 60], with milder assumptions in shallow networks [10, 43]. However, the convexity of our CGNNs enables global optimality and computational efficiency without relying on any of the above restrictive assumptions.

Convex Neural Networks. The area of convex neural networks is relatively underexplored. Zhang et al. [57] proposed a convex relaxation step for fully-connected neural networks, which inspired the convexification of convolutional neural networks (CNNs) [59]. Other works study linear CNNs [19] and linear GNNs [41], which are of less interest in practice since they collapse all layers into one. Recently, Cohen and Agmon [6] proposed convex versions of specific GNN models termed as aggregation GNN, which apply only to a signal with temporal structure [15]. Their work is narrowly tailored and focused on a specific application in swarm robotics, where convexity arises from modeling assumptions tailored to domain adaptation. In contrast, our CGNN framework establishes a general and theoretically principled convexification of diverse message-passing GNNs by transforming the standard architecture itself, independent of application-specific constraints. Unlike their formulation that does not preserve, e.g., standard GNN modularity, our approach retains these key structural features and applies broadly to a wide range of graph learning tasks. As such, CGNNs represent a scalable and domain-agnostic foundation for convex GNN training, grounded in a fundamentally different mathematical framework.

Graph Transformers. Instead of aggregating local neighborhood, Graph Transformers capture interaction information between any pair of nodes via a single self-attention layer. Some works design specific attention mechanisms or positional encodings [21, 25, 28, 52], while others combine message-passing GNNs to build hybrid architectures [5, 36, 40, 49]. Those methods enable nodes to interact with any other node, facilitating direct modeling of long-range relations. Our framework broadly applies to such hybrid methods, as we exhibit on the leading models GraphGPS [36] and GraphTrans [40, 49]. Empirically, applying our framework consistently improves performance in graph classification tasks, with significant gains on GraphGPS, showcasing the versatility and effectiveness of our approach.

Notations. For brevity, $[n]$ denotes the discrete set $\{1, 2, \dots, n\}$ for any $n \in \mathbb{N}_{>0}$. For a rectangular matrix A , let $\|A\|_*$ be its nuclear norm (i.e., the sum of A 's singular values), and $\|A\|_2$ be its spectral norm (i.e., maximal singular value). Let $\ell^2(\mathbb{N})$ be the set of countable dimensional of square-summable sequences v , i.e., $\sum_{i=1}^{\infty} v_i^2 < \infty$.

3 Preliminaries

Network data can be captured by an underlying undirected graph $\mathcal{G} = (\mathcal{V}, \mathcal{E}, \mathcal{W})$, where $\mathcal{V} = \{1, \dots, n\}$ denotes the vertex set, \mathcal{E} denotes the edge set and $\mathcal{W} : \mathcal{E} \rightarrow \mathbb{R}$ denotes the edge weight function, while a missing edge (i, j) is depicted by $\mathcal{W}(i, j) = 0$. The *neighborhood* of node $i \in \mathcal{V}$ is denoted by $N_i := \{j \in \mathcal{V} | (j, i) \in \mathcal{E}\}$. The data on top of this graph is modeled as a *graph signal* $\mathcal{X} \in \mathbb{R}^{n \times F}$, whose i^{th} row $[\mathcal{X}]_i = \mathbf{x}_i$ is an F -dimensional *feature vector* assigned to node $i \in \mathcal{V}$. We leverage the framework of *graph signal processing* (GSP) [33] as the mathematical foundation for learning from graph signals. For relating the graph signal \mathcal{X} with the underlying structure of \mathcal{G} , we define

a *graph shift operator* (GSO) by $\mathcal{S} \in \mathbb{R}^{n \times n}$, which satisfies $[\mathcal{S}]_{ij} = s_{ij} = 0$ if $(j, i) \notin \mathcal{E}$ for $j \neq i$. Commonly utilized GSOs include the **adjacency** matrix [37, 38], the **Laplacian** matrix [42], and their normalized counterparts [7, 16]. By viewing \mathcal{S} as a linear operator, the graph signal \mathcal{X} can be *shifted* over the nodes, yielding that the output at node i for the f^{th} feature becomes $[\mathcal{S}\mathcal{X}]_{if} = \sum_{j=1}^n [\mathcal{S}]_{ij} [\mathcal{X}]_{jf} = \sum_{j \in N_i} s_{ij} x_{jf}$. Note that, whereas $\mathcal{S}\mathcal{X}$ corresponds to a local information exchange between a given node and its direct neighbors, applying this linear operator recursively aggregates information from nodes in further hops along the graph. Namely, the k -shifted signal $\mathcal{S}^k \mathcal{X}$ aggregates information from nodes that are k -hops away.

Graph Convolutional Networks (GCNs) [17] stack multiple graph (convolutional) layers to extract high-level node representations from graph signals. To formally describe the creation of convolutional features in a GCN with $L \in \mathbb{N}$ layers, let the output of layer $\ell - 1$ (and thus the input to the ℓ^{th} layer) be $\mathcal{X}_{\ell-1}$, comprising of $F_{\ell-1}$ feature vectors. The input to layer 0 is $\mathcal{X}_0 = \mathcal{X}$, yielding $F_0 = F$, while the final output has $G := F_L$ features. Given a set of *filters* $A := \{\mathcal{A}_{\ell k} \in \mathbb{R}^{F_{\ell-1} \times F_{\ell}} | k \in [K] \cup \{0\}, \ell \in [L]\}$, the *graph (convolutional) filter* at layer ℓ processes the $F_{\ell-1}$ features of the input graph signal $\mathcal{X}_{\ell-1}$ in parallel by F_{ℓ} graph filters to output the following F_{ℓ} convolutional features:

$$\Psi^{\mathcal{A}_{\ell}}(\mathcal{X}; \mathcal{S}) := \sum_{k=0}^K \mathcal{S}^k \mathcal{X}_{\ell-1} \mathcal{A}_{\ell k}, \quad (1)$$

where $\mathcal{A}_{\ell} := (\mathcal{A}_{\ell k})_{k=0}^K$ concatenates the filters at layer ℓ . Note that all nodes share the same parameters to weigh equally the information from all k -hop away neighbors for any $k \in [K]$, which corresponds to the *parameter sharing* of GCNs. A GCN is then defined as a nonlinear mapping between graph signals $\Phi : \mathbb{R}^{n \times F} \rightarrow \mathbb{R}^{n \times G}$, which is obtained by feeding the aggregated features through a pointwise nonlinear activation function $\sigma : \mathbb{R} \rightarrow \mathbb{R}$ (which, for brevity, denotes its entrywise application in (2)), producing the feature vectors of the ℓ^{th} layer's output:

$$\Phi(\mathcal{X}; \mathcal{S}, A) := \mathcal{X}_L; \quad \mathcal{X}_{\ell} := \sigma(\Psi^{\mathcal{A}_{\ell}}(\mathcal{X}; \mathcal{S})). \quad (2)$$

We denote the f^{th} column of the filters $\mathcal{A}_{\ell k}$ as $\mathbf{a}_{\ell k}^f = [a_{\ell k}^{fg}]_{g \in [F_{\ell-1}]}$. Given some positive constants $\{R_{\ell}\}_{\ell \in [L]}$, we consider the following *non-convex* function class of (regularized) GCNs:

$$\mathcal{F}_{\text{gcn}} := \{\Phi \text{ as in (2)} : \max_{0 \leq k \leq K} \|\mathbf{a}_{\ell k}^f\|_2 \leq R_{\ell} \forall f, \ell\}. \quad (3)$$

By setting $R_{\ell} = \infty$ for any $\ell \in [L]$, this function class reduces to the class of (unregularized) GCNs.

3.1 Training GCNs

We focus on the *graph classification* task with G classes. Here, we are given a training set $\mathcal{T} := \{(\mathcal{G}^{(j)}, \mathcal{X}^{(j)}, y^{(j)})\}_{j=1}^m$ of m samples, where the j^{th} sample consists of a graph $\mathcal{G}^{(j)}$, a graph signal $\mathcal{X}^{(j)} \in \mathbb{R}^{n \times F}$ over $\mathcal{G}^{(j)}$ and the graph's true label $y^{(j)} \in [G]$. Without loss of generality, we assume that each graph $\mathcal{G}^{(j)}$ has n nodes (otherwise, we can add isolated dummy nodes). We then train a GCN (as formulated in (2)), while node features from the last layer are aggregated to obtain the graph-level representation via a permutation invariant function, such as summation or a more sophisticated graph-level pooling function [54, 56]. Training is done by solving the following optimization problem for some loss function $J : \mathbb{R}^{n \times G} \times \mathbb{R}^n \rightarrow \mathbb{R}$:

$$\Phi_{\text{gcn}}^* \in \arg \min_{\Phi \in \mathcal{F}_{\text{gcn}}} \frac{1}{m} \sum_{j=1}^m J(\Phi(\mathcal{X}^{(j)}; \mathcal{S}, A), y^{(j)}). \quad (4)$$

We assume that J is convex and M -Lipschitz in its first argument (predictions) for any fixed second argument (labels). The number of parameters to be trained are determined by the number of layers L , the number of filters K and features F_ℓ in each layer ℓ . By (2), each GCN $\Phi \in \mathcal{F}_{\text{gcn}}$ depends nonlinearly on the parameters, making the optimization problem in (4) non-convex. Next, we thus present a relaxation of the class \mathcal{F}_{gcn} , enabling a convex formulation of the associated problem in (4).

4 Convexification of GCNs

As \mathcal{F}_{gcn} in (3) is a non-convex set and the activation function is nonlinear, the ERM problem on GCNs is non-convex, raising the challenges mentioned in Section 1. To overcome them, we propose a procedure for making both the ERM’s predictions domain and loss function *convex*. Following Zhang et al. [59], we develop the class of **Convexified GCNs (CGCNs)**. In Section 4.1, we first depict our method for *linear* activation functions. Given that the linear activation function would collapse all layers into one, this case is of no interest in practice. However, it supplies us with some insight into the general kernelization scheme of GCNs. In the nonlinear case (Section 4.2), we reduce the problem to the linear case by proposing a relaxation to a suitably chosen *Reproducing Kernel Hilbert Space* (RKHS), enabling us to obtain a convex formulation of the associated ERM problem. We then present an algorithm for learning CGCNs (Section 4.3), discuss its scalability and time complexity (Section 4.4), and establish its generalization guarantees (Section 4.5).

4.1 Convexification of GCNs with *Linear* Activation Functions

To provide the intuition for our method, we employ the nuclear norm in the simple case of the linear activation function $\sigma(\mathbf{w}) = \mathbf{w}$, which provides us with a convex function class, as opposed to (3). In this case, the output of layer ℓ is simply $\mathcal{X}_\ell = \sum_{k=0}^K \mathcal{S}^k \mathcal{X}_{\ell-1} \mathcal{A}_{\ell k}$ due to (1)-(2). Hence, \mathcal{X}_ℓ linearly depends on the filters $\{\mathcal{A}_{\ell k}\}_{k=0}^K$ of layer ℓ , i.e., the convolution function $\Psi^{\mathcal{A}_\ell} : \mathbb{R}^{n \times F_{\ell-1}} \rightarrow \mathbb{R}^{n \times F_\ell}$ in (1) linearly depends on the parameters.

Low-Rank Constraints. The filters matrix $\mathcal{A}_{\ell k} \in \mathbb{R}^{F_{\ell-1} \times F_\ell}$ has rank at most $F_{\ell-1}$. As $\mathcal{A}_\ell := (\mathcal{A}_{\ell k})_{k=0}^K$ concatenates the filters at layer ℓ , then $\text{rank}(\mathcal{A}_\ell) \leq F_{\ell-1}$. Hence, the class \mathcal{F}_{gcn} of GCNs in (3) corresponds to a collection of functions depending on norm and low-rank constraints imposed on the filters. We next define:

$$\mathcal{F}_{\text{linear-gcn}} := \{\Psi^{\mathcal{A}_\ell} : \max_{0 \leq k \leq K} \|\mathbf{a}_{\ell k}^f\|_2 \leq R_\ell \quad \text{and} \quad (5a)$$

$$\text{rank}(\mathcal{A}_\ell) = F_{\ell-1} \quad \forall f, \ell\}, \quad (5b)$$

which is the specific form of our original class of GCNs in (3) for the linear case. While (5a) holds even when the parameters are *not* shared over all nodes, the low-rank constraint (5b) will no longer be satisfied in this case. Namely, (5b) is achieved via GCNs’ parameter sharing: each node processes its neighborhood up to K hops away using the same filters, and thus the number of independent rows of parameters remains at most $F_{\ell-1}$, regardless of the number of nodes in the graph.

Nuclear Norm Relaxation. However, filters that satisfy the constraints (5a) and (5b) form a *non-convex* set. A standard convex relaxation of a rank constraint involves replacing it with a nuclear norm constraint. That is, controlling the sum of singular values instead of the number of non-zero ones, similarly to how the ℓ_1 -c can be viewed as a convex relaxation of the ℓ_0 -norm constraint.

Upper Bounding the Nuclear-Norm. In Appendix A, we prove that:

Lemma 4.1. *Assume that the filters \mathcal{A}_ℓ at each layer ℓ satisfy (5a) and (5b). Then, \mathcal{A}_ℓ 's nuclear norm is upper bounded as $\|\mathcal{A}_\ell\|_* \leq \mathcal{B}_\ell$ for some $\mathcal{B}_\ell > 0$ that is a function of $R_\ell, F_\ell, F_{\ell-1}, K$.*

Using Lemma 4.1, we can replace (5a) and (5b) with a nuclear norm constraint, thus forming a convex function class. Namely, we define the class of **Convexified GCNs** (CGCNs) as:

$$\mathcal{F}_{\text{cgcn}} := \{\{\Psi^{\mathcal{A}_\ell}\}_{\ell=1}^L : \|\mathcal{A}_\ell\|_* \leq \mathcal{B}_\ell \quad \forall \ell\}, \quad (6)$$

while guaranteeing that $\mathcal{F}_{\text{gcn}} \subseteq \mathcal{F}_{\text{cgcn}}$. Thus, solving the ERM in (4) over $\mathcal{F}_{\text{cgcn}}$ instead of \mathcal{F}_{gcn} yields a convex optimization problem over a wealthier class of functions. Next, for the more general setting of *nonlinear* activation functions, we devise an algorithm capable of solving this convex program.

4.2 Convexification of GCNs with *Nonlinear* Activation Functions

For certain nonlinear activation functions σ and suitably chosen kernel function κ such as the Gaussian RBF kernel, we next prove how the class \mathcal{F}_{gcn} of GCNs in (3) can be relaxed to a *Reproducing Kernel Hilbert Space* (RKHS), reducing the problem to the linear activation case (Readers may refer to [39] for a brief overview on RKHS). Beforehand, we rephrase the filter at layer ℓ from (1)-(2) as follows. Denoting the f^{th} column of the filters $\mathcal{A}_{\ell k}$ as $\mathbf{a}_{\ell k}^f$, in Appendix C we prove that:

Lemma 4.2. *A GCN induces a nonlinear filter τ_ℓ^f at each layer ℓ for the f^{th} feature given as follows (where the activation function σ is applied entrywise):*

$$\tau_\ell^f : \mathcal{Z} \in \mathbb{R}^{(K+1) \times F_{\ell-1}} \mapsto \sigma(\sum_{k=0}^K \langle [\mathcal{Z}]_{k+1}, \mathbf{a}_{\ell k}^f \rangle). \quad (7)$$

For any graph signal $\mathcal{S}^k \mathcal{X}$, let $\mathbf{z}_i^k(\mathcal{X}) := [\mathcal{S}^k \mathcal{X}]_i$ be the i^{th} row of $\mathcal{S}^k \mathcal{X}$, which is the information aggregated at node i from k -hops away. Defining the matrix $\mathcal{Z}_{i,\ell}(\mathcal{X}_{\ell-1}) \in \mathbb{R}^{(K+1) \times F_{\ell-1}}$ whose $(k+1)^{\text{th}}$ row is $[\mathcal{Z}_{i,\ell}(\mathcal{X}_{\ell-1})]_{k+1} = \mathbf{z}_i^k(\mathcal{X}_{\ell-1})$ for $k \in [K] \cup \{0\}$, the output at layer ℓ is thus given by $\tau_\ell^k(\mathcal{Z}_{i,\ell}(\mathcal{X}_{\ell-1}))$.

Kernelization of GCNs. In the sequel, we consider a training data $\mathcal{T} = \{(\mathcal{G}^{(j)}, \mathcal{X}^{(j)}, y^{(j)})\}_{j=1}^m$, some layer of index ℓ and a positive semi-definite kernel function $\kappa_\ell : \mathbb{R}^{F_{\ell-1}} \times \mathbb{R}^{F_{\ell-1}} \rightarrow \mathbb{R}$ for layer ℓ . Thus, for brevity, we omit indices involving ℓ and $\mathcal{X}_{\ell-1}^{(j)}$ when no ambiguity arises. Namely, we denote, e.g., $\mathcal{Z}_{i,j} := \mathcal{Z}_{i,\ell}(\mathcal{X}_{\ell-1}^{(j)})$ and $\mathbf{z}_{i,j}^k := \mathbf{z}_i^k(\mathcal{X}_{\ell-1}^{(j)})$.

First, we prove in Lemma 4.3 that the filter specified by (7) resides in the RKHS induced by the kernel (See Appendix D for a proof, which adapts the one by Zhang et al. [59] to GCNs). Zhang et al. [59] prove that convolutional neural networks can be contained within the RKHS induced by properly chosen kernel and activation functions. For certain choices of kernels (e.g., the Gaussian RBF kernel) and a sufficiently smooth σ (e.g., smoothed hinge loss), we can similarly prove that the filter τ_ℓ^f in (7) is contained within the RKHS induced by the kernel function κ_ℓ . See Appendices B.1-B.2 for possible choices of kernels and Appendix B.3 for valid activation functions, as well as an elaboration on sufficient smoothness in Remark B.2.

Lemma 4.3. *The filter τ_ℓ^f at layer ℓ for the f^{th} feature can be reparametrized as a linear combination of kernel products, reducing the problem to the linear activations case. Formally:*

$$\tau_\ell^f(\mathcal{Z}_{i,j}) = \sum_{k=0}^K \sum_{(i',j') \in [n] \times [m]} \alpha_{k,(i',j')}^f \cdot \kappa_\ell(\mathbf{z}_{i,j}^k, \mathbf{z}_{i',j'}^k), \quad (8)$$

where $\{\alpha_{k,(i',j')}^f\}_{(i',j',k) \in [n] \times [m] \times ([K] \cup \{0\})}$ are some coefficients.

Remark 4.4. *Lemma 4.3 suggests that filters of the form (8) are parameterized by a finite set of coefficients $\{\alpha_{k,(i',j')}^f\}$, allowing optimization to be carried over these coefficients instead of the original parameters \mathcal{A}_ℓ (See Section 4.3 for details on solving this optimization problem).*

To avoid re-deriving all results in the kernelized setting, we reduce the problem to the linear case in Section 4.1. Thus, consider the (symmetric) kernel matrix $\mathcal{K}_\ell^k \in \mathbb{R}^{nm \times nm}$, whose entry at row (i, j) and column (i', j') equals to $\kappa_\ell(\mathbf{z}_{i,j}^k, \mathbf{z}_{i',j'}^k)$. We factorize the kernel matrix as $\mathcal{K}_\ell^k = Q_\ell^k (Q_\ell^k)^\top$, where $Q_\ell^k \in \mathbb{R}^{nm \times P}$ (as in [59], we can use, e.g., Cholesky factorization [8] with $P = nm$).

Remark 4.5. *The (i, j) -th row of Q_ℓ^k , i.e., $\mathbf{q}_{i,j}^k := [Q_\ell^k]_{(i,j)} \in \mathbb{R}^P$, can be interpreted as a feature vector instead of the original $\mathbf{z}_{i,j}^k \in \mathbb{R}^{F_{\ell-1}}$ (the information aggregated at node i from k -hops away).*

Thus, the reparameterization in (8) of the filter at layer ℓ for the f^{th} feature can be rephrased as:

$$\tau_\ell^f(\mathcal{Z}_{i,j}) = \sum_{k=0}^K \langle \mathbf{q}_{i,j}^k, \hat{\mathbf{a}}_{\ell k}^f \rangle; \quad \hat{\mathbf{a}}_{\ell k}^f := \sum_{(i',j',k) \in [n] \times [m] \times ([K] \cup \{0\})} \alpha_{k,(i',j')}^f \mathbf{q}_{i',j'}^k \quad (9)$$

Next, we outline the learning and testing phases of CGCNs (See Appendix D for more details).

Remark 4.6. *Relaxing the filters to the induced RKHS reduces the problem to the linear case. The resulting relaxed filters satisfy a low-rank constraint and have a bounded nuclear norm. By Section 4.1, convexly relaxing the low-rank constraint via the nuclear norm yields a convex function class.*

To summarize, we describe the forward pass operation of a single layer in Algorithm 1. It processes an input graph signal \mathcal{X} and transforms it in two steps:

Step 1: Arranging Input to the Layer. Each layer ℓ takes as input the graph signal $\mathcal{X}_{\ell-1}$ from the previous layer and computes intermediate graph signals $Z_\ell^k(\mathcal{X}_{\ell-1})$ for different hop distances k (line 2). For each node i , information is aggregated from its k -hop neighbors (line 4), from which the i^{th} row of $Z_\ell^k(\mathcal{X}_{\ell-1})$ is then obtained based on kernel products (lines 4-6).

Step 2: Computing the Layer Output. Using the intermediate representations and the trainable filters $\hat{\mathcal{A}}_{\ell k}$, the layer's output signal \mathcal{X}_ℓ is calculated (line 8). Specifically, each node's output feature vector at layer ℓ is computed via a weighted sum of the transformed signals (line 9).

4.3 The Algorithm for Learning Multi-Layer CGCNs

Algorithm 2 summarizes the training process of a multi-layer CGCN, estimating the parameters of each layer from bottom to top (i.e., in a layer-wise fashion). As such, to learn the nonlinear filter τ_ℓ^f at layer ℓ , we should learn the P -dimensional vector $\hat{\mathbf{a}}_{\ell k}^f$. For this sake, we define the graph signal $Z_j^k \in \mathbb{R}^{n \times P}$ for any $k \in [K] \cup \{0\}$ and $j \in [m]$ whose i^{th} row is $[Q_\ell^k]_{(i,j)}$. We can then apply

Algorithm 1 Forward Pass of the ℓ^{th} CGCN Layer

Input: Graph signal $\mathcal{X} \in \mathbb{R}^{n \times F}$, filters $\hat{\mathcal{A}}_\ell = (\hat{\mathcal{A}}_{\ell k})_{k=0}^K$

- 1: **Step 1: Arrange input to layer ℓ**
- 2: Given an input graph signal $\mathcal{X}_{\ell-1} \in \mathbb{R}^{n \times F}$ from the previous layer, compute a new graph signal $Z_\ell^k(\mathcal{X}_{\ell-1}) \in \mathbb{R}^{n \times P}$ for any $\ell \in [L]$ and $k \in [K] \cup \{0\}$ as follows.
- 3: Compute $\mathbf{z}_i^k(\mathcal{X}_{\ell-1}^{(j)}) := [\mathcal{S}^k \mathcal{X}_{\ell-1}^{(j)}]_i$, the signal aggregated at node i from k -hops away with respect to the training graph signal $\mathcal{X}^{(j)}$.
- 4: As usual in kernel methods, we need to compute $\kappa_\ell(\mathbf{z}, \mathbf{z}_i^k(\mathcal{X}_{\ell-1}))$, where $\mathbf{z} \in \mathbb{R}^{n \times F}$ is some input graph signal.
- 5: Form the vector $\mathbf{v}_\ell^k(\mathbf{z}_i^k(\mathcal{X}_{\ell-1}))$ whose elements are kernel products (See Appendix D).
- 6: Compute the i^{th} row of $Z_\ell^k(\mathcal{X}_{\ell-1})$ using $Z_\ell^k(\mathcal{X}_{\ell-1})_i = (Q^k)^\dagger \mathbf{v}_\ell^k(\mathbf{z}_i^k(\mathcal{X}_{\ell-1}))$, where $(Q^k)^\dagger$ is the pseudo-inverse of Q^k (See Appendix D for more details).
- 7: **Step 2: Compute the layer's output**
- 8: Using the computed signals $Z_\ell^k(\mathcal{X}_{\ell-1})$, construct the output graph signal \mathcal{X}_ℓ for layer ℓ .
- 9: Layer ℓ induces a *linear* mapping between graph signals $\hat{\Psi}^{\hat{\mathcal{A}}_\ell} : \mathbb{R}^{n \times F_{\ell-1}} \rightarrow \mathbb{R}^{n \times F_\ell}$ s.t. the value of the f^{th} feature of node i at layer ℓ is $[\mathcal{X}_\ell]_{if} = [\hat{\Psi}^{\hat{\mathcal{A}}_\ell}(\mathcal{X}_{\ell-1})]_{if} = \sum_{k=0}^K \langle \hat{\mathbf{z}}_i^k(\mathcal{X}_{\ell-1}), \hat{\mathbf{a}}_{\ell k}^f \rangle$, where $\hat{\mathbf{a}}_{\ell k}^f$ are the trainable parameters (filters) of the CGCN layer from (9).

Output: Output graph signal $\mathcal{X}_\ell \in \mathbb{R}^{n \times F_\ell}$

Algorithm 2 Training of CGCNs

Input: Training set $\mathcal{T} = \{(\mathcal{G}^{(j)}, \mathcal{X}^{(j)}, y^{(j)})\}_{j=1}^m$; Kernels $\{\kappa_\ell\}_{\ell=1}^L$; Regularization parameters $\{\mathcal{B}_\ell\}_{\ell=1}^L$; Number of graph filters $\{F_\ell\}_{\ell=1}^L$

- 1: **for each** layer $2 \leq \ell \leq L$ **do**
- 2: Taking $\{(\mathcal{G}^{(j)}, \mathcal{X}_{\ell-1}^{(j)}, y^{(j)})\}_{j=1}^m$ as training samples, construct a kernel matrix $\mathcal{K}_\ell^k \in \mathbb{R}^{nm \times nm}$ as in Section 4.2.
- 3: Compute a factorization or an approximation of \mathcal{K}_ℓ^k to obtain $Q_\ell^k \in \mathbb{R}^{nm \times P}$.
- 4: For any sample $\mathcal{X}_{\ell-1}^{(j)}$, form a graph signal $Z_\ell^k(\mathcal{X}_{\ell-1}^{(j)}) \in \mathbb{R}^{n \times P}$ via line 6 of Algorithm 1.
- 5: Solve (10) via (11) to obtain the filters $\hat{\mathcal{A}}_\ell$.
- 6: Compute the output $\mathcal{X}_\ell^{(j)}$ of layer ℓ via Algorithm 1.

Output: Predictors $\{\hat{\Psi}^{\hat{\mathcal{A}}_\ell}(\cdot)\}_{\ell=1}^L$ and the output $\mathcal{X}_L^{(j)}$.

the nuclear norm relaxation from Section 4.1. Solving the resulting optimization problem yields a matrix of filters $\hat{\mathcal{A}}_{\ell k} \in \mathbb{R}^{P \times F_\ell}$ for layer ℓ whose f^{th} column is $\hat{\mathbf{a}}_{\ell k}^f$.

Given regularization parameters $\{\mathcal{B}_\ell\}_{\ell=1}^L$ for the filters' nuclear norms, we thus aim to solve the following optimization problem at each layer ℓ due to line 9 of Algorithm 1:

$$\hat{\mathcal{A}}_\ell \in \arg \min_{\|\hat{\mathcal{A}}_\ell\|_* \leq \mathcal{B}_\ell} \tilde{J}(\hat{\mathcal{A}}_\ell), \quad \text{where } \tilde{J}(\hat{\mathcal{A}}_\ell) := \frac{1}{m} \sum_{j=1}^m J(\hat{\Psi}^{\hat{\mathcal{A}}_\ell}(\mathcal{X}_{\ell-1}^{(j)}), y^{(j)}). \quad (10)$$

This can be easily solved via *projected gradient descent*: at round t , with step size $\eta^t > 0$, compute:

$$\hat{\mathcal{A}}_\ell^{t+1} = \Pi_{\mathcal{B}_\ell}(\hat{\mathcal{A}}_\ell^t - \eta^t \nabla_{\hat{\mathcal{A}}_\ell} \tilde{J}(\hat{\mathcal{A}}_\ell^t)) \quad (11)$$

where $\nabla_{\hat{\mathcal{A}}_\ell} \tilde{J}$ is the gradient of \tilde{J} from (10) and $\Pi_{\mathcal{B}_\ell}$ denotes the Euclidean projection onto the nuclear norm ball $\{\hat{\mathcal{A}}_\ell : \|\hat{\mathcal{A}}_\ell\|_* \leq \mathcal{B}_\ell\}$. This projection can be done by first computing the singular value decomposition of $\hat{\mathcal{A}}_\ell$ and then projecting the vector of singular values onto the ℓ_1 -ball via an efficient algorithm (see, e.g., [13, 12, 50]). The problem in (10) can also be solved using a projected version of any other optimizer (e.g., Adam [23]).

4.4 Scalability, Time Complexity and Challenges of Learning CGCNs

Algorithm 2's runtime highly depends on how the factorization matrix Q_ℓ^k is computed and its width P (line 3). Naively picking $P = nm$ requires solving the exact kernelized problem, which can be costly. To gain scalability, we compute a *Nystrom approximation* [48] in $\mathcal{O}(P^2nm)$ time by randomly sampling training examples, computing their kernel matrix and representing each training example by its similarity to the sampled examples and kernel matrix. This avoids computing or storing the full kernel matrix, thus requiring only $\mathcal{O}(Pmn)$ space. While this approach is efficient [48, 9], it relies on the sampled subset adequately representing the entire data; poorly represented examples may degrade approximation quality. See Appendix E for more details and alternative methods.

4.5 Convergence and Generalization Error

We now analyze Algorithm 2's generalization error, focusing on models with a single hidden layer ($L = 1$) in the binary classification case where the output dimension is $G = 1$. Our main result can be easily extended to the multi-class case by a standard one-versus-all reduction to the binary case. In case of multiple hidden layers, our analysis then applies to each hidden layer separately. Specifically, by an approach similar to Zhang et al. [59], we prove that the generalization error of Algorithm 2 converges to the optimal generalization error of a GCN, as it is bounded above by this optimal error plus an additive term that decays polynomially to zero with the sample size. For any $\ell \in [L]$ and $k \in [K]$, we use the random kernel matrix $\mathcal{K}_\ell^k(\mathcal{X}) \in \mathbb{R}^{n \times n}$ induced by a graph signal $\mathcal{X} \in \mathbb{R}^{n \times F}$ drawn randomly from the population, i.e., the (i, i') -th entry of $\mathcal{K}_\ell^k(\mathcal{X})$ is $\kappa_\ell(\mathbf{z}_i^k(\mathcal{X}), \mathbf{z}_{i'}^k(\mathcal{X}))$, where $\mathbf{z}_i^k(\mathcal{X}_{\ell-1}) := [\mathcal{S}^k \mathcal{X}_{\ell-1}]_i$ aggregates information at node i from k -hops away.

Theorem 4.7. *Consider models with a single hidden layer for binary classification (i.e., $L = G = 1$). Let $J(\cdot, \mathbf{y})$ be M -Lipchitz continuous for any fixed $\mathbf{y} \in [G]^n$ and let κ_L be either the inverse polynomial kernel or the Gaussian RBF kernel (Recall Appendices B.1-B.2). For any valid activation function σ (Recall Appendix B.3), there is a constant radius $R_L > 0$ such that the expected generalization error is at most:*

$$\mathbb{E}_{\mathcal{X}, \mathbf{y}}[J(\hat{\Psi}^{\hat{\mathcal{A}}_L}(\mathcal{X}), \mathbf{y})] \leq \inf_{\Phi \in \mathcal{F}_{\text{gcn}}} \mathbb{E}_{\mathcal{X}, \mathbf{y}}[J(\Phi(\mathcal{X}), \mathbf{y})] + \frac{\text{Const}}{\sqrt{m}},$$

where Const is some constant that depends on R_L , but not on the sample size m .

Proof. (Sketch) The full proof in Appendix F comprises of two steps: When $L = G = 1$, we first consider a wealthier function class, denoted as $\mathcal{F}_{\text{cgcn}}$, which is proven to contain the class of GCNs \mathcal{F}_{gcn} from (2). The richer class relaxes the class of GCNs in two aspects: (1) The graph filters are relaxed to belong to the RKHS induced by the kernel, and (2) the ℓ_2 -norm constraints in (2) are substituted by a single constraint on the Hilbert norm induced by the kernel. Though Algorithm 2 never explicitly optimizes over the function class $\mathcal{F}_{\text{cgcn}}$, we prove that the predictor $\hat{\Psi}^{\hat{\mathcal{A}}_L}$ generated at the last layer is an empirical risk minimizer in $\mathcal{F}_{\text{cgcn}}$. Then, we prove that $\mathcal{F}_{\text{cgcn}}$ is not "too big"

by upper bounding its *Rademacher complexity*, a key concept in empirical process theory that can be used to bound the generalization error in our ERM problem (see, e.g., [2] for a brief overview on Rademacher complexity). Combining this upper bound with standard Rademacher complexity theory [2], we infer that the generalization error of $\hat{\Psi}^{\hat{\mathcal{A}}_L}$ converges to the best generalization error of \mathcal{F}_{gcn} . Since $\mathcal{F}_{\text{gcn}} \subset \mathcal{F}_{\text{cgcn}}$, the latter error is bounded by that of GCNs, completing the proof. \square

5 Experimental Evaluation

Datasets. We evaluate our framework through extensive experiments on several benchmark graph classification datasets [31], including the four bioinformatics datasets MUTAG, PROTEINS, PTC-MR, NCI1 and the chemical compounds dataset Mutagenicity. Following many prior works [29, 53], we randomly split each dataset into three parts: 80% as training set, 10% as validation set and the remaining 10% as test set. The statistics of these datasets appear in Appendix G.1.

Baselines. We apply our convexification procedure to the message-passing mechanisms of popular GNNs and hybrid graph transformers, creating convex counterparts. Our framework is integrated into a wide range of leading models, including GCN [7, 24], GAT [45], GATv2 [4], GIN [51], GraphSAGE [20], ResGatedGCN [3], as well as the hybrid transformers GraphGPS [36] and GraphTrans [40, 49]. All models share the same architecture design for fair comparison; see Appendix G.2 for details.

Optimization. All models are trained over 200 epochs with the Adam optimizer [23] using the cross entropy loss, a starting learning rate of 10^{-3} , a minimum learning rate of 10^{-6} and a weight decay of 10^{-5} . We use a ReduceLROnPlateau scheduler, which cuts the learning rate in half with a patience of 20 epochs, and training ends when we reach the minimum learning rate.

Results and Analysis. Table 1 presents our main empirical results, comparing two-layer convex models against two-layer and six-layer non-convex models. Impressively, in most cases, the two-layer convex variants substantially surpass their non-convex counterparts by 10–40% accuracy, showcasing the practical strength of our framework alongside its theoretical benefits. Even when improvements are modest, our convex models match or slightly surpass their non-convex versions, underscoring the robustness and broad applicability of our approach. Notable examples are GATv2 and GraphGPS, whose convex versions significantly outperform their non-convex ones in 4 out of 5 datasets, with slight improvements on Mutagenicity. Our convex models’ superiority over the hybrid transformer GraphGPS, which combines message-passing with self-attention, highlights the power of convexified GNNs over non-convex ones, even when enhanced by self-attention. To visualize these trends more holistically, we also include additional plots in Appendix H.

Over-parameterization is known to aid gradient-based methods to reach global minima that generalize well in non-convex models [1, 11, 60], making it a common practice for obtaining strong performance. Our results challenge this approach. We show that our shallow convex models often outperform their more over-parameterized non-convex counterparts, obtaining better results with fewer layers and parameters. In effect, we beat them twice: in performance and in resource efficiency. These gains are especially notable in small-data regimes, which are prone to overfitting, where we suspect that local optima obtained by non-convex models may hinder generalization. In contrast, convex models avoid such pitfalls, offering more stable and reliable learning. Our findings show that rich representations can be attained without over-parameterization by exploiting convexity in shallow models.

Table 1: Accuracy ($\% \pm \sigma$) of two-layer convex versions of base models against their two-layer and six-layer non-convex counterparts on various graph classification datasets over 4 runs, each with different seeds. The datasets are ordered from left to right in ascending order of size. Convex variants start with 'C'. A two-layer model is marked by (2L), while a six-layer one is marked by (6L). Results of convex models surpassing their non-convex variants by a large gap ($\sim 10\text{-}40\%$) are in **dark green** and modest improvements in **light green**.

Model	MUTAG	PTC-MR	PROTEINS	NCI1	Mutagenicity
CGCN (2L)	71.2 \pm 2.1	59.7 \pm 4.2	70.9 \pm 2.4	62.3 \pm 1.1	61.9 \pm 2.7
GCN (2L)	55.0 \pm 22.0	48.5 \pm 10.4	59.5 \pm 4.1	50.8 \pm 1.7	54.7 \pm 1.1
GCN (6L)	61.2 \pm 21.6	55.0 \pm 15.8	58.7 \pm 6.1	50.8 \pm 1.7	54.7 \pm 1.9
CGIN (2L)	83.2 \pm 7.3	63.2 \pm 4.7	70.1 \pm 2.6	63.6 \pm 2.3	59.1 \pm 1.8
GIN (2L)	60.0 \pm 17.6	45.0 \pm 9.5	50.4 \pm 12.0	55.5 \pm 1.4	54.8 \pm 2.0
GIN (6L)	61.2 \pm 1.6	48.5 \pm 13.4	61.6 \pm 1.2	60.8 \pm 2.8	55.8 \pm 2.0
CGAT (2L)	72.5 \pm 4.7	59.7 \pm 6.0	71.8 \pm 2.5	64.6 \pm 0.0	58.8 \pm 3.6
GAT (2L)	65.0 \pm 9.3	51.4 \pm 15.7	60.0 \pm 3.3	51.9 \pm 2.2	54.8 \pm 2.0
GAT (6L)	68.7 \pm 4.1	54.2 \pm 17.2	63.1 \pm 1.8	52.3 \pm 2.9	54.8 \pm 2.0
CGATv2 (2L)	68.7 \pm 4.1	59.0 \pm 5.2	71.3 \pm 0.6	63.6 \pm 1.1	62.3 \pm 4.2
GATv2 (2L)	55.0 \pm 19.0	49.2 \pm 15.3	61.6 \pm 1.6	49.5 \pm 2.0	55.9 \pm 1.4
GATv2 (6L)	57.5 \pm 16.0	49.2 \pm 15.3	63.3 \pm 2.1	49.5 \pm 2.0	59.6 \pm 6.2
CResGatedGCN (2L)	68.7 \pm 4.1	60.4 \pm 5.8	72.5 \pm 1.0	62.4 \pm 3.2	59.6 \pm 3.7
ResGatedGCN (2L)	57.0 \pm 16.7	50.7 \pm 17.7	47.9 \pm 9.9	56.8 \pm 6.6	56.1 \pm 2.1
ResGatedGCN (6L)	65.0 \pm 15.8	50.7 \pm 7.1	55.8 \pm 8.7	61.1 \pm 3.1	56.1 \pm 2.1
CGraphSAGE (2L)	68.7 \pm 4.1	65.3 \pm 11.5	73.8 \pm 3.7	63.7 \pm 1.0	66.3 \pm 5.3
GraphSAGE (2L)	57.4 \pm 16.0	52.8 \pm 7.4	62.5 \pm 0.8	53.1 \pm 6.0	58.1 \pm 3.6
GraphSAGE (6L)	51.2 \pm 1.9	55.7 \pm 12.5	63.1 \pm 1.8	53.2 \pm 6.1	60.0 \pm 3.3
CGraphTrans (2L)	68.7 \pm 4.1	63.3 \pm 10.8	70.7 \pm 3.1	63.1 \pm 2.8	63.2 \pm 4.7
GraphTrans (2L)	57.4 \pm 16.0	40.4 \pm 8.0	60.7 \pm 2.6	55.0 \pm 3.7	53.6 \pm 1.3
GraphTrans (6L)	67.5 \pm 7.4	49.2 \pm 12.3	61.6 \pm 1.2	61.5 \pm 2.5	59.9 \pm 4.6
CGraphGPS (2L)	83.7 \pm 2.1	65.5 \pm 9.3	81.6 \pm 7.2	60.1 \pm 6.1	59.4 \pm 4.1
GraphGPS (2L)	50.9 \pm 19.6	49.2 \pm 20.1	38.0 \pm 1.9	50.8 \pm 2.6	41.4 \pm 8.7
GraphGPS (6L)	52.5 \pm 2.1	46.4 \pm 2.3	38.8 \pm 1.5	49.4 \pm 1.9	55.1 \pm 5.5

6 Conclusions and Future Work

We presented Convexified Message-Passing Graph Neural Networks (CGNNs), a novel framework that transforms the training of message-passing GNNs to a convex optimization problem. They ensure global optimality and computational efficiency, while having provable generalization and statistical guarantees. Empirically, we demonstrated that our CGNNs framework can effectively capture complex patterns without the need for over-parameterization or extensive data. This insight offers a more efficient and data-scarce alternative to traditional deep learning approaches, with substantial improvements across various benchmark datasets. As discussed in Section 4.4, the

training of CGNNs is heavily affected by the factorization of the kernel matrix in terms of time and space complexity. Addressing these challenges is thus a key direction for future work.

References

- [1] Zeyuan Allen-Zhu, Yuanzhi Li, and Zhao Song. A convergence theory for deep learning via over-parameterization. In *International conference on machine learning*, pages 242–252. PMLR, 2019.
- [2] Peter L Bartlett and Shahar Mendelson. Rademacher and gaussian complexities: Risk bounds and structural results. *Journal of Machine Learning Research*, 3:463–482, 2002.
- [3] Xavier Bresson and Thomas Laurent. Residual gated graph convnets. *arXiv preprint arXiv:1711.07553*, 2017.
- [4] Shaked Brody, Uri Alon, and Eran Yahav. How attentive are graph attention networks? In *International Conference on Learning Representations*, 2022.
- [5] Dexiong Chen, Leslie O’Bray, and Karsten Borgwardt. Structure-aware transformer for graph representation learning. In *International Conference on Machine Learning*, volume 162, pages 3469–3489, 2022.
- [6] Saar Cohen and Noa Agmon. Convexified graph neural networks for distributed control in robotic swarms. In *International Joint Conferences on Artificial Intelligence Organization*, pages 2307–2313, 2021.
- [7] Michaël Defferrard, Xavier Bresson, and Pierre Vandergheynst. Convolutional neural networks on graphs with fast localized spectral filtering. *Advances in neural information processing systems*, 29:3844–3852, 2016.
- [8] Dariusz Dereniowski and Marek Kubale. Cholesky factorization of matrices in parallel and ranking of graphs. In *International Conference on Parallel Processing and Applied Mathematics*, pages 985–992. Springer, 2003.
- [9] Petros Drineas and Michael W Mahoney. Approximating a gram matrix for improved kernel-based learning. In *International Conference on Computational Learning Theory*, pages 323–337. Springer, 2005.
- [10] Simon Du and Jason Lee. On the power of over-parametrization in neural networks with quadratic activation. In *International conference on machine learning*, pages 1329–1338. PMLR, 2018.
- [11] Simon S Du, Xiyu Zhai, Barnabas Poczos, and Aarti Singh. Gradient descent provably optimizes over-parameterized neural networks. In *International Conference on Learning Representations*, 2018.
- [12] John Duchi, Elad Hazan, and Yoram Singer. Adaptive subgradient methods for online learning and stochastic optimization. *Journal of Machine Learning Research*, 12(61):2121–2159, 2011.

- [13] John Duchi, Shai Shalev-Shwartz, Yoram Singer, and Tushar Chandra. Efficient projections onto the ℓ_1 -ball for learning in high dimensions. In *Proceedings of the 25th international conference on Machine learning*, pages 272–279, 2008.
- [14] Matthias Fey and Jan Eric Lenssen. Fast graph representation learning with PyTorch Geometric. *arXiv preprint arXiv:1903.02428*, 2019.
- [15] Fernando Gama, Antonio G Marques, Geert Leus, and Alejandro Ribeiro. Convolutional neural network architectures for signals supported on graphs. *IEEE Transactions on Signal Processing*, 67(4):1034–1049, 2018.
- [16] Fernando Gama, Alejandro Ribeiro, and Joan Bruna. Diffusion scattering transforms on graphs. In *International Conference on Learning Representations*, 2019.
- [17] Fernando Gama, Alejandro Ribeiro, and Joan Bruna. Stability of graph scattering transforms. *Advances in Neural Information Processing Systems*, 32, 2019.
- [18] Justin Gilmer, Samuel S Schoenholz, Patrick F Riley, Oriol Vinyals, and George E Dahl. Neural message passing for quantum chemistry. In *International conference on machine learning*, pages 1263–1272. PMLR, 2017.
- [19] Suriya Gunasekar, Jason D Lee, Nathan Srebro, and Daniel Soudry. Implicit bias of gradient descent on linear convolutional networks. *Advances in Neural Information Processing Systems*, 31:9461–9471, 2018.
- [20] Will Hamilton, Zhitao Ying, and Jure Leskovec. Inductive representation learning on large graphs. In *Advances in Neural Information Processing Systems*, volume 30, 2017.
- [21] Md Shamim Hussain, Mohammed J Zaki, and Dharmashankar Subramanian. Global self-attention as a replacement for graph convolution. In *ACM SIGKDD Conference on Knowledge Discovery and Data Mining*, pages 655–665, 2022.
- [22] John Ingraham, Vikas K Garg, Regina Barzilay, and Tommi Jaakkola. Generative models for graph-based protein design. In *Proceedings of the 33rd International Conference on Neural Information Processing Systems*, volume 32, pages 15820–15831, 2019.
- [23] Diederik P Kingma and Jimmy Ba. Adam: A method for stochastic optimization. In *International Conference on Learning Representations*, 2015.
- [24] Thomas N. Kipf and Max Welling. Semi-supervised classification with graph convolutional networks. In *International Conference on Learning Representations*, 2017.
- [25] Devin Kreuzer, Dominique Beaini, Will Hamilton, Vincent Létourneau, and Prudencio Tossou. Rethinking graph transformers with spectral attention. *Advances in Neural Information Processing Systems*, 34:21618–21629, 2021.
- [26] Quoc Le, Tamas Sarlos, and Alexander Smola. Fastfood - computing hilbert space expansions in loglinear time. In *International Conference on Machine Learning*, volume 28, pages 244–252, 2013.
- [27] Yang Li, Buyue Qian, Xianli Zhang, and Hui Liu. Graph neural network-based diagnosis prediction. *Big data*, 8(5):379–390, 2020.

- [28] Liheng Ma, Chen Lin, Derek Lim, Adriana Romero-Soriano, Puneet K Dokania, Mark Coates, Philip Torr, and Ser-Nam Lim. Graph inductive biases in transformers without message passing. In *International Conference on Machine Learning*, pages 23321–23337. PMLR, 2023.
- [29] Yao Ma, Suhang Wang, Charu C Aggarwal, and Jiliang Tang. Graph convolutional networks with eigenpooling. In *ACM SIGKDD international conference on knowledge discovery & data mining*, pages 723–731, 2019.
- [30] Stanislav Minsker. On some extensions of bernstein’s inequality for self-adjoint operators. *Statistics & Probability Letters*, 127:111–119, 2017.
- [31] Christopher Morris, Nils Morten Kriege, Franka Bause, Kristian Kersting, Petra Mutzel, and Marion Neumann. Tudataset: A collection of benchmark datasets for learning with graphs. In *ICML 2020 Workshop on Graph Representation Learning and Beyond (GRL+ 2020)*, 2020. www.graphlearning.io.
- [32] Christopher Morris, Martin Ritzert, Matthias Fey, William L Hamilton, Jan Eric Lenssen, Gaurav Rattan, and Martin Grohe. Weisfeiler and leman go neural: Higher-order graph neural networks. *Proceedings of the AAAI conference on artificial intelligence*, 33(01):4602–4609, 2019.
- [33] Antonio Ortega, Pascal Frossard, Jelena Kovačević, José MF Moura, and Pierre Vandergheynst. Graph signal processing: Overview, challenges, and applications. *Proceedings of the IEEE*, 106(5):808–828, 2018.
- [34] Adam Paszke, Sam Gross, Francisco Massa, Adam Lerer, James Bradbury, Gregory Chanan, Trevor Killeen, Zeming Lin, Natalia Gimelshein, Luca Antiga, Alban Desmaison, Andreas Kopf, Edward Yang, Zachary DeVito, Martin Raison, Alykhan Tejani, Sasank Chilamkurthy, Benoit Steiner, Lu Fang, Junjie Bai, and Soumith Chintala. Pytorch: An imperative style, high-performance deep learning library. In H. Wallach, H. Larochelle, A. Beygelzimer, F. d’Alché-Buc, E. Fox, and R. Garnett, editors, *Advances in Neural Information Processing Systems*, volume 32, pages 8024–8035, 2019.
- [35] Ali Rahimi and Benjamin Recht. Random features for large-scale kernel machines. In *Advances in neural information processing systems*, volume 20, pages 1177–1184, 2007.
- [36] Ladislav Rampášek, Michael Galkin, Vijay Prakash Dwivedi, Anh Tuan Luu, Guy Wolf, and Dominique Beaini. Recipe for a general, powerful, scalable graph transformer. *Advances in Neural Information Processing Systems*, 35:14501–14515, 2022.
- [37] Aliaksei Sandryhaila and José MF Moura. Discrete signal processing on graphs. *IEEE transactions on signal processing*, 61(7):1644–1656, 2013.
- [38] Aliaksei Sandryhaila and Jose MF Moura. Discrete signal processing on graphs: Frequency analysis. *IEEE Transactions on Signal Processing*, 62(12):3042–3054, 2014.
- [39] Bernhard Schölkopf, Ralf Herbrich, and Alex J Smola. A generalized representer theorem. In *International conference on computational learning theory*, pages 416–426. Springer, 2001.
- [40] Yunsheng Shi, Zhengjie Huang, Shikun Feng, Hui Zhong, Wenjing Wang, and Yu Sun. Masked label prediction: Unified message passing model for semi-supervised classification. In *International Joint Conferences on Artificial Intelligence Organization*, pages 1548–1554, 2021.

- [41] Seiyun Shin, Ilan Shomorony, and Han Zhao. Efficient learning of linear graph neural networks via node subsampling. *Advances in Neural Information Processing Systems*, 36:55479–55501, 2023.
- [42] David I Shuman, Sunil K Narang, Pascal Frossard, Antonio Ortega, and Pierre Vandergheynst. The emerging field of signal processing on graphs: Extending high-dimensional data analysis to networks and other irregular domains. *IEEE signal processing magazine*, 30(3):83–98, 2013.
- [43] Mahdi Soltanolkotabi, Adel Javanmard, and Jason D Lee. Theoretical insights into the optimization landscape of over-parameterized shallow neural networks. *IEEE Transactions on Information Theory*, 65(2):742–769, 2018.
- [44] Ingo Steinwart. *Support Vector Machines*. Springer, 2008.
- [45] Petar Veličković, Guillem Cucurull, Arantxa Casanova, Adriana Romero, Pietro Liò, and Yoshua Bengio. Graph attention networks. In *International Conference on Learning Representations*, 2018.
- [46] Oriol Vinyals, Samy Bengio, and Manjunath Kudlur. Order matters: Sequence to sequence for sets. *International Conference on Learning Representations*, 2015.
- [47] Zhouxia Wang, Tianshui Chen, Jimmy Ren, Weihao Yu, Hui Cheng, and Liang Lin. Deep reasoning with knowledge graph for social relationship understanding. In *International Joint Conference on Artificial Intelligence*, pages 1021–1028, 2018.
- [48] Christopher KI Williams and Matthias Seeger. Using the nyström method to speed up kernel machines. In *Advances in neural information processing systems*, pages 682–688, 2001.
- [49] Zhanghao Wu, Paras Jain, Matthew Wright, Azalia Mirhoseini, Joseph E Gonzalez, and Ion Stoica. Representing long-range context for graph neural networks with global attention. *Advances in neural information processing systems*, 34:13266–13279, 2021.
- [50] Lin Xiao and Tong Zhang. A proximal stochastic gradient method with progressive variance reduction. *SIAM Journal on Optimization*, 24(4):2057–2075, 2014.
- [51] Keyulu Xu, Weihua Hu, Jure Leskovec, and Stefanie Jegelka. How powerful are graph neural networks? In *International Conference on Learning Representations*, 2019.
- [52] Chengxuan Ying, Tianle Cai, Shengjie Luo, Shuxin Zheng, Guolin Ke, Di He, Yanming Shen, and Tie-Yan Liu. Do transformers really perform badly for graph representation? *Advances in neural information processing systems*, 34:28877–28888, 2021.
- [53] Rex Ying, Ruining He, Kaifeng Chen, Pong Eksombatchai, William L Hamilton, and Jure Leskovec. Graph convolutional neural networks for web-scale recommender systems. In *Proceedings of the 24th ACM SIGKDD international conference on knowledge discovery & data mining*, pages 974–983, 2018.
- [54] Zhitao Ying, Jiaxuan You, Christopher Morris, Xiang Ren, Will Hamilton, and Jure Leskovec. Hierarchical graph representation learning with differentiable pooling. *Advances in neural information processing systems*, 31, 2018.

- [55] Yuning You, Tianlong Chen, Yang Shen, and Zhangyang Wang. Graph contrastive learning automated. In *International conference on machine learning*, pages 12121–12132. PMLR, 2021.
- [56] Muhan Zhang, Zhicheng Cui, Marion Neumann, and Yixin Chen. An end-to-end deep learning architecture for graph classification. *Proceedings of the AAAI conference on artificial intelligence*, 32(1), 2018.
- [57] Yuchen Zhang, Jason D. Lee, and Michael I. Jordan. ℓ_1 -regularized neural networks are improperly learnable in polynomial time. In *International Conference on Machine Learning*, volume 48, pages 993–1001, 2016.
- [58] Yuchen Zhang, Jason D Lee, and Michael I Jordan. ℓ_1 -regularized neural networks are improperly learnable in polynomial time. In *International Conference on Machine Learning*, pages 993–1001, 2016.
- [59] Yuchen Zhang, Percy Liang, and Martin J Wainwright. Convexified convolutional neural networks. In *International Conference on Machine Learning*, pages 4044–4053. PMLR, 2017.
- [60] Difan Zou, Yuan Cao, Dongruo Zhou, and Quanquan Gu. Gradient descent optimizes over-parameterized deep relu networks. *Machine learning*, 109:467–492, 2020.

A Upper Bounding the Nuclear Norm

Lemma 4.1. *For any layer ℓ , $\|\mathcal{A}_\ell\|_* \leq \mathcal{B}_\ell$ for some constant $\mathcal{B}_\ell > 0$ dependent on $R_\ell, F_\ell, F_{\ell-1}, K$.*

Proof. Note that the nuclear norm of any matrix B can be bounded as $\|B\|_* \leq \|B\|_F \sqrt{\text{rank}(B)}$, where $\|B\|_F$ is the Frobenius norm which is identical to the standard Euclidean norm of the vectorized version of the matrix. Hence, the nuclear norm of the filters \mathcal{A}_ℓ satisfying (5a) and (5b) is upper bounded by

$$\|\mathcal{A}_\ell\|_*^2 \leq \|\mathcal{A}_\ell\|_F^2 F_{\ell-1} = \sum_{k=0}^K \sum_{f \in [F_\ell]} \sum_{g \in [F_{\ell-1}]} |a_{\ell k}^{fg}|^2 \cdot F_{\ell-1} \leq R_\ell^2 F_\ell F_{\ell-1} (K+1).$$

That is, $\|\mathcal{A}_\ell\|_* \leq \mathcal{B}_\ell$ for $\mathcal{B}_\ell := R_\ell \sqrt{F_\ell F_{\ell-1} (K+1)}$. □

B Choice of Kernels and Valid Activations

In this section, we provide properties regarding two types of kernels: the *inverse polynomial kernel* (Section B.1) and the *Gaussian RBF kernel* (Section B.2). We show that the reproducing kernel Hilbert space (RKHS) corresponding to these kernels contain the nonlinear filter at each layer ℓ for the f^{th} feature of node i for certain choices of an activation function σ . Finally, we summarize the possible choices for an activation function σ that result from our discussion (Section B.3).

B.1 Inverse Polynomial Kernel

For F features, the *inverse polynomial kernel* $\kappa^{IP} : \mathbb{R}^F \times \mathbb{R}^F \rightarrow \mathbb{R}$ is given as follows:

$$\kappa^{IP}(\mathbf{z}, \mathbf{z}') := \frac{1}{2 - \langle \mathbf{z}, \mathbf{z}' \rangle}; \quad \|\mathbf{z}\|_2 \leq 1, \|\mathbf{z}'\|_2 \leq 1 \quad (12)$$

Zhang et al. [59] prove that κ^{IP} indeed constitutes a legal kernel function. We include the proof to make the paper self-contained: they provide a feature mapping $\varphi : \mathbb{R}^F \rightarrow \ell^2(\mathbb{N})$ for which $\kappa^{IP}(\mathbf{z}, \mathbf{z}') = \langle \varphi(\mathbf{z}), \varphi(\mathbf{z}') \rangle$. The (k_1, \dots, k_j) -th coordinate of $\varphi(\mathbf{z})$, where $j \in \mathbb{N}$ and $k_1, \dots, k_j \in [F]$, is given by $2^{-\frac{j+1}{2}} x_{k_1} \dots x_{k_j}$. Thus:

$$\langle \varphi(\mathbf{z}), \varphi(\mathbf{z}') \rangle = \sum_{j=0}^{\infty} 2^{-(j+1)} \sum_{(k_1, \dots, k_j) \in [F]_j} z_{k_1} \dots z_{k_j} z'_{k_1} \dots z'_{k_j} \quad (13)$$

Since $\|\mathbf{z}\|_2 \leq 1$ and $\|\mathbf{z}'\|_2 \leq 1$, the series above is absolutely convergent. Combined with the fact that $|\langle \mathbf{z}, \mathbf{z}' \rangle| \leq 1$, this yields a simplified form of (13):

$$\langle \varphi(\mathbf{z}), \varphi(\mathbf{z}') \rangle = \sum_{j=0}^{\infty} 2^{-(j+1)} (\langle \mathbf{z}, \mathbf{z}' \rangle)^j = \frac{1}{2 - \langle \mathbf{z}, \mathbf{z}' \rangle} = \kappa^{IP}(\mathbf{z}, \mathbf{z}') \quad (14)$$

as desired. Combining (7) with the proof of Lemma 1 in Appendix A.1 of Zhang et al. [58], the RKHS associated with κ^{IP} is comprised of the class of nonlinear graph filters in (7). It can be formulated as follows:

Corollary B.1. *Assume that σ has a polynomial expansion $\sigma(t) = \sum_{j=0}^{\infty} a_j t^j$. Let $C_{\sigma}(t) := \sqrt{\sum_{j=0}^{\infty} 2^{j+1} a_j^2 t^{2j}}$. If $C_{\sigma}(\|\mathbf{a}_{\ell k}^f\|_2) < \infty$, then the RKHS induced by κ^{IP} contains the function $\tau_{\ell}^f : \mathcal{Z} \in \mathbb{R}^{(K+1) \times F_{\ell-1}} \mapsto \sigma(\sum_{k=0}^K \langle [\mathcal{Z}]_{k+1}, \mathbf{a}_{\ell k}^f \rangle)$ with Hilbert norm $\|\tau_{\ell}^f\|_A \leq C_{\sigma}(\sum_{k=0}^K \|\mathbf{a}_{\ell k}^f\|_2)$.*

Consequently, Zhang et al. [58] state that upper bounding $C_{\sigma}(t)$ for a particular activation function σ is sufficient. To enforce $C_{\sigma}(t) < \infty$, the scalars $\{a_j\}_{j=0}^{\infty}$ must rapidly converge to zero, implying that σ must be sufficiently smooth. For polynomial functions of degree d , the definition of C_{σ} yields $C_{\sigma}(t) = \mathcal{O}(t^d)$. For the *sinusoid* activation $\sigma(t) := \sin(t)$, we have:

$$C_{\sigma}(t) = \sqrt{\sum_{j=0}^{\infty} \frac{2^{2j+2}}{((2j+1)!)^2} (t^2)^{2j+1}} \leq 2e^{t^2} \quad (15)$$

For the *erf* function $\sigma_{\text{erf}}(t) := \frac{2}{\sqrt{\pi}} \int_0^t e^{-z^2} dz$ and the *smoothed hinge loss* function $\sigma_{\text{sh}}(t) := \int_{-\infty}^t \frac{1}{2} (\sigma_{\text{erf}}(t) + 1) dz$, Zhang et al. [58] proved that $C_{\sigma}(t) = \mathcal{O}(e^{ct^2})$ for universal numerical constant $c > 0$.

Remark B.2. *Generally, a function f is **sufficiently smooth** if it is differentiable sufficient number of times. For instance, if we were to consider $\sigma(t) := \sin(t)$, its Taylor expansion is provided by $\sin(t) = \sum_{j=0}^{\infty} \frac{(-1)^j}{(2j+1)!} t^{2j+1}$. Denoting $b_j := \frac{(-1)^j}{(2j+1)!} t^{2j+1}$, the ratio test yields $\lim_{j \rightarrow \infty} |\frac{b_{j+1}}{b_j}| = 0$ for all $t \in \mathbb{R}$. Hence, the radius of convergence of the expansion is the set of all real numbers.*

Regarding Corollary B.1, as well as Corollary B.3 which follows in the next subsection, for enforcing $C_{\sigma}(t) < \infty$, the coefficients $\{a_j\}_{j=0}^{\infty}$ in σ 's polynomial expansion must quickly converge to zero as illustrated above, thus requiring σ to be sufficiently smooth. Such activations include **polynomial functions**, the **sinusoid**, the **erf** function and the **smoothed hinge loss**.

B.2 Gaussian RBF Kernel

For F features, the *Gaussian RBF kernel* $\kappa^{RBF} : \mathbb{R}^F \times \mathbb{R}^F \rightarrow \mathbb{R}$ is given as follows:

$$\kappa^{RBF}(\mathbf{z}, \mathbf{z}') := e^{-\gamma \|\mathbf{z} - \mathbf{z}'\|_2^2}; \quad \|\mathbf{z}\|_2 = \|\mathbf{z}'\|_2 = 1 \quad (16)$$

Combining (7) with the proof of Lemma 2 in Appendix A.2 of Zhang et al. [58], the RKHS associated with κ^{RBF} is comprised of the class of nonlinear input features. It can be formulated as follows:

Corollary B.3. *Assume that σ has a polynomial expansion $\sigma(t) = \sum_{j=0}^{\infty} a_j t^j$. Let $C_\sigma(t) := \sqrt{\sum_{j=0}^{\infty} \frac{j! e^{2\gamma}}{(2\gamma)^j} a_j^2 t^{2j}}$. If $C_\sigma(\|\mathbf{a}_{\ell k}^f\|_2) < \infty$, then the RKHS induced by κ^{RBF} contains the function $\tau_\ell^f : \mathcal{Z} \in \mathbb{R}^{(K+1) \times F_{\ell-1}} \mapsto \sigma(\sum_{k=0}^K \langle [\mathcal{Z}]_{k+1}, \mathbf{a}_{\ell k}^f \rangle)$ with Hilbert norm $\|\tau_\ell^f\|_A \leq C_\sigma(\sum_{k=0}^K \|\mathbf{a}_{\ell k}^f\|_2)$.*

Comparing Corollary B.1 and Corollary B.3, κ^{RBF} requires a stronger condition on the smoothness of the activation function. For polynomial functions of degree d , $C_\sigma(t) = \mathcal{O}(t^d)$ remains intact. However, for the *sinusoid* activation $\sigma(t) := \sin(t)$, we have:

$$C_\sigma(t) = \sqrt{e^{2\gamma} \sum_{j=0}^{\infty} \frac{1}{(2j+1)!} \left(\frac{t^2}{2\gamma}\right)^{2j+1}} \leq e^{\frac{t^2}{4\gamma} + \gamma} \quad (17)$$

In contrast, for both the *erf* function $\sigma_{erf}(t) := \frac{2}{\sqrt{\pi}} \int_0^t e^{z^2} dz$ and the *smoothed hinge loss* function $\sigma_{sh}(t) := \int_{-\infty}^t \frac{1}{2}(\sigma_{erf}(\tau) + 1)d\tau$, $C_\sigma(t)$ is **infinite**. Hence, **the RKHS induced by κ^{RBF} does not contain input features activated by those two functions.**

B.3 Valid Activation Functions

Now, we summarize the possible valid choices of an activation function σ :

1. Arbitrary polynomial functions.
2. The sinusoid activation function $\sigma(t) := \sin(t)$.
3. The *erf* function $\sigma_{erf}(t) := \frac{2}{\sqrt{\pi}} \int_0^t e^{\tau^2} d\tau$, which approximates the sigmoid function.
4. The *smoothed hinge loss* function $\sigma_{sh}(t) := \int_{-\infty}^t \frac{1}{2}(\sigma_{erf}(\tau) + 1)d\tau$, which approximates the ReLU function.

Recall that the *erf* and *smoothed hinge loss* activation functions are unsuited for the RBF kernel.

C Rephrasing the Nonlinear Filter at each Layer

Proof. For any graph signal $\mathcal{S}^k \mathcal{X}$, let $\mathbf{z}_i^k(\mathcal{X}) := [\mathcal{S}^k \mathcal{X}]_i$ be the i^{th} row of $\mathcal{S}^k \mathcal{X}$, which is the information aggregated at node i from k -hops away. We also denote the f^{th} column of the filters $\mathcal{A}_{\ell k}$ as $\mathbf{a}_{\ell k}^f = [a_{\ell k}^{fg}]_{g \in [F_{\ell-1}]}$. By (1), the value of the f^{th} feature of node i at layer ℓ can be thus written as:

$$[\Psi^{\mathcal{A}_\ell}(\mathcal{X}; \mathcal{S})]_{if} = \sum_{k=0}^K \sum_{g=1}^{F_{\ell-1}} [\mathbf{z}_i^k(\mathcal{X}_{\ell-1})]_g [\mathbf{a}_{\ell k}^f]_g = \sum_{k=0}^K \langle \mathbf{z}_i^k(\mathcal{X}_{\ell-1}), \mathbf{a}_{\ell k}^f \rangle. \quad (18)$$

Defining the matrix $\mathcal{Z}_{i,\ell}(\mathcal{X}_{\ell-1}) \in \mathbb{R}^{(K+1) \times F_{\ell-1}}$ whose $(k+1)^{\text{th}}$ row is $[\mathcal{Z}_{i,\ell}(\mathcal{X}_{\ell-1})]_{k+1} = \mathbf{z}_i^k(\mathcal{X}_{\ell-1})$ for $k \in [K] \cup \{0\}$, \square

D Kernelization for Nonlinear Activations

In this section, we elaborate on the kernelization for the case of nonlinear activation functions, briefly discussed in Section 4.2. Recall that σ denotes, for brevity, its entrywise application in (2). Further, the f^{th} feature of node i at layer ℓ 's output is given by $\sigma(\sum_{k=0}^K \langle \mathbf{z}_i^k(\mathcal{X}_{\ell-1}), \mathbf{a}_{\ell k}^f \rangle)$ by (18). According to Appendix B, consider a sufficiently smooth valid activation function σ , and a proper choice of kernel $\kappa_\ell : \mathbb{R}^{F_{\ell-1}} \times \mathbb{R}^{F_{\ell-1}} \rightarrow \mathbb{R}$. Without loss of generality, we assume that, each input graph signal $\mathcal{X}^{(j)}$, the feature vector $[\mathcal{X}^{(j)}]_i = \mathbf{x}_i^{(j)}$ of each node i resides in the unit ℓ_2 -ball (which can be obtained via normalization). Combined with κ_ℓ 's being a continuous kernel with $\kappa_\ell(\mathbf{z}, \mathbf{z}) \leq 1$, Mercer's theorem [44, Theorem 4.49] implies that there exists a feature mapping $\varphi_\ell : \mathbb{R}^{F_{\ell-1}} \rightarrow \ell^2(\mathbb{N})$ for which $\kappa_\ell(\mathbf{z}, \mathbf{z}') = \langle \varphi_\ell(\mathbf{z}), \varphi_\ell(\mathbf{z}') \rangle$, which yields the following for each feature f of any node i at layer ℓ :

$$\sigma\left(\sum_{k=0}^K \langle \mathbf{z}_i^k(\mathcal{X}_{\ell-1}), \mathbf{a}_{\ell k}^f \rangle\right) = \sum_{k=0}^K \langle \varphi_\ell(\mathbf{z}_i^k(\mathcal{X}_{\ell-1})), \varphi_\ell(\mathbf{a}_{\ell k}^f) \rangle =: \sum_{k=0}^K \langle \varphi_\ell(\mathbf{z}_i^k(\mathcal{X}_{\ell-1})), \bar{\mathbf{a}}_{\ell k}^f \rangle \quad (19)$$

where $\bar{\mathbf{a}}_{\ell k}^f \in \ell^2(\mathbb{N})$ is a countable-dimensional vector, due to the fact that φ itself is a countable sequence of functions. By Corollary B.1 and Corollary B.3, we have that $\|\bar{\mathbf{a}}_{\ell k}^f\|_2 \leq C_{\sigma, \ell}(\|\mathbf{a}_{\ell k}^f\|_2)$, provided a monotonically increasing C_σ which depends on the kernel κ_ℓ . Accordingly, $\varphi_\ell(\mathbf{z})$ may be utilized as the vectorized representation of each output features $\mathbf{z}_i^k(\mathcal{X}_{\ell-1})$, where $\bar{\mathbf{a}}_{\ell k}^f$ constitutes the linear graph filters, thus reducing the problem to training a GCN with the identity activation function.

Each graph filter is now parametrized by the *countable*-dimensional vector $\bar{\mathbf{a}}_{\ell k}^f$. Subsequently, we supply a reduction of the original ERM problem to a *finite*-dimensional one. Output on the training data $\mathcal{T} := \{(\mathcal{G}^{(j)}, \mathcal{X}^{(j)}, y^{(j)})\}_{j=1}^m$ should be solely considered when solving the ERM problem, i.e., $\sum_{k=0}^K \langle \varphi_\ell(\mathbf{z}_i^k(\mathcal{X}_{\ell-1})), \bar{\mathbf{a}}_{\ell k}^f \rangle$ for each feature f of any node i at layer ℓ . Let $\mathcal{P}_{\ell-1}^k$ be the orthogonal projector onto the linear subspace spanned by $\Gamma_{\ell-1}^k := \{\mathbf{z}_i^k(\mathcal{X}_{\ell-1}^{(j)}) : i \in [n], j \in [m], k \in [K] \cup \{0\}\}$. Therefore, for any $(i, j) \in [n] \times [m]$:

$$\sum_{k=0}^K \langle \varphi_\ell(\mathbf{z}_i^k(\mathcal{X}_{\ell-1}^{(j)})), \bar{\mathbf{a}}_{\ell k}^f \rangle = \sum_{k=0}^K \langle \mathcal{P}_{\ell-1}^k \varphi_\ell(\mathbf{z}_i^k(\mathcal{X}_{\ell-1}^{(j)})), \bar{\mathbf{a}}_{\ell k}^f \rangle = \sum_{k=0}^K \langle \varphi_\ell(\mathbf{z}_i^k(\mathcal{X}_{\ell-1}^{(j)})), \mathcal{P}_{\ell-1}^k \bar{\mathbf{a}}_{\ell k}^f \rangle \quad (20)$$

where the last step stems from the fact that the orthogonal projector $\mathcal{P}_{\ell-1}^k$ is self-adjoint. Without loss of generality, for the sake of solving the ERM, we assume that $\bar{\mathbf{a}}_{\ell k}^f$ belongs to $\Gamma_{\ell-1}^k$. Similarly to (8), we can thus reparameterize it by:

$$\bar{\mathbf{a}}_{\ell k}^f = \sum_{(i, j) \in [n] \times [m]} \beta_{\ell k, (i, j)}^f \varphi_\ell(\mathbf{z}_i^k(\mathcal{X}_{\ell-1}^{(j)})) \quad (21)$$

where we denote $\beta_{\ell k}^f \in \mathbb{R}^{nm}$ as a vector of the coefficients, whose (i, j) -th coordinate is $\beta_{\ell k, (i, j)}^f$. To estimate $\bar{\mathbf{a}}_{\ell k}^f$, it thus suffices to estimate the vector $\beta_{\ell k}^f$. By definition, the relation $(\beta_{\ell k}^f)^T \mathcal{K}_\ell^k \beta_{\ell k}^f = \|\bar{\mathbf{a}}_{\ell k}^f\|_2^2$ holds, where $\mathcal{K}_\ell^k \in \mathbb{R}^{nm \times nm}$ is the symmetric kernel matrix from Section 4.2, whose rows and columns are indexed by some triple $(i, j) \in [n] \times [m]$. The entry at row (i, j) and column (i', j') equals to $\kappa_\ell(\mathbf{z}_i^k(\mathcal{X}_{\ell-1}^{(j)}), \mathbf{z}_{i'}^k(\mathcal{X}_{\ell-1}^{(j')}))$. A suitable factorization of \mathcal{K}_ℓ^k such that $\mathcal{K}_\ell^k = Q_\ell^k (Q_\ell^k)^\top$

for $Q_\ell^k \in \mathbb{R}^{nm \times P}$ then yields the following norm constraint:

$$\|(Q_\ell^k)^\top \beta_{\ell k}^f\|_2 = \sqrt{(\beta_{\ell k}^f)^\top \mathcal{K}_\ell^k \beta_{\ell k}^f} = \|\bar{\mathbf{a}}_{\ell k}^f\|_2^2 \leq C_{\sigma, \ell}(\|\mathbf{a}_{\ell k}^f\|_2) \leq C_{\sigma, \ell}(R_\ell) \quad (22)$$

where the last inequality is due to $\|\mathbf{a}_{\ell k}^f\|_2 \leq R_\ell$ due to (3).

Let $\mathbf{v}_\ell^k(\mathbf{z}) \in \mathbb{R}^{nm}$ be a vector whose (i, j) -th coordinate equals to $\kappa_\ell(\mathbf{z}, \mathbf{z}_i^k(\mathcal{X}_{\ell-1}^{(j)}))$. By (19) and (21), we can write:

$$\begin{aligned} \sigma \left(\sum_{k=0}^K \langle \mathbf{z}_i^k(\mathcal{X}_{\ell-1}^{(j)}), \bar{\mathbf{a}}_{\ell k}^f \rangle \right) &\equiv \sum_{k=0}^K \langle \varphi_\ell(\mathbf{z}_i^k(\mathcal{X}_{\ell-1}^{(j)})), \bar{\mathbf{a}}_{\ell k}^f \rangle \equiv \sum_{k=0}^K \langle \mathbf{v}_\ell^k(\mathbf{z}_i^k(\mathcal{X}_{\ell-1}^{(j)})), \beta_{\ell k}^f \rangle \\ &\equiv \sum_{k=0}^K \langle \beta_{\ell k}^f, \mathbf{v}_\ell^k(\mathbf{z}_i^k(\mathcal{X}_{\ell-1}^{(j)})) \rangle \end{aligned} \quad (23)$$

For each $\mathbf{z}_i^k(\mathcal{X}_{\ell-1}^{(j)})$, the vector $\mathbf{v}_\ell^k(\mathbf{z}_i^k(\mathcal{X}_{\ell-1}^{(j)}))$ resides in the column space of the symmetric kernel matrix \mathcal{K}_ℓ^k . Thus, given that $(Q_\ell^k)^\dagger$ denotes the pseudo-inverse of Q_ℓ^k , we infer the following for any $(i, j) \in [n] \times [m]$:

$$\begin{aligned} \sum_{k=0}^K \langle \beta_{\ell k}^f, \mathbf{v}_\ell^k(\mathbf{z}_i^k(\mathcal{X}_{\ell-1}^{(j)})) \rangle &= \sum_{k=0}^K (\beta_{\ell k}^f)^\top Q_\ell^k (Q_\ell^k)^\dagger \mathbf{v}_\ell^k(\mathbf{z}_i^k(\mathcal{X}_{\ell-1}^{(j)})) \\ &= \sum_{k=0}^K \left\langle ((Q_\ell^k)^\top)^\dagger (Q_\ell^k)^\top \beta_{\ell k}^f, \mathbf{v}_\ell^k(\mathbf{z}_i^k(\mathcal{X}_{\ell-1}^{(j)})) \right\rangle \end{aligned} \quad (24)$$

Accordingly, replacing the vector $\beta_{\ell k}^f$ on the right-hand side of (23) by $((Q_\ell^k)^\top)^\dagger (Q_\ell^k)^\top \beta_{\ell k}^f$ won't affect the empirical risk. For any matrix $\mathcal{Z} \in \mathbb{R}^{(K+1) \times F_{\ell-1}}$ whose $(k+1)$ th row is given by $[\mathcal{Z}]_{k+1} := \mathbf{z}_k$ for $k \in [K] \cup \{0\}$, we thereby propose the following parameterization function:

$$\tau_\ell^f(\mathcal{Z}) := \sum_{k=0}^K \left\langle ((Q_\ell^k)^\top)^\dagger (Q_\ell^k)^\top \beta_{\ell k}^f, \mathbf{v}_\ell^k(\mathbf{z}_k) \right\rangle = \sum_{k=0}^K \langle (Q_\ell^k)^\dagger \mathbf{v}_\ell^k(\mathbf{z}_k), (Q_\ell^k)^\top \beta_{\ell k}^f \rangle \quad (25)$$

Consequently, the value of the f^{th} feature of node i at layer ℓ is given by $\tau_\ell^f(\mathcal{Z}_{i, \ell}(\mathcal{X}_{\ell-1}))$, where $\mathcal{Z}_{i, \ell}(\mathcal{X}_{\ell-1}) \in \mathbb{R}^{(K+1) \times F_{\ell-1}}$ is the matrix whose $(k+1)$ th row is $[\mathcal{Z}_{i, \ell}(\mathcal{X}_{\ell-1})]_k = \mathbf{z}_i^k(\mathcal{X}_{\ell-1})$ for $k \in [K] \cup \{0\}$. That is, $(Q_\ell^k)^\top \beta_{\ell k}^f$ now act as the filters under the reparameterization in (25) which satisfy the following constraints:

Norm Constraint. $\|(Q_\ell^k)^\top \beta_{\ell k}^f\|_2 \leq C_{\sigma, \ell}(R_\ell)$ due to (22).

Rank Constraint. Its rank is at most $F_{\ell-1}$.

Therefore, similarly to the linear case in Section 4.1, those constraints can be relaxed to the nuclear norm constraint:

$$\|(Q_\ell^k)^\top \beta_{\ell k}^f\|_* \leq C_{\sigma, \ell}(R_\ell) \sqrt{F_\ell F_{\ell-1} (K+1)} \quad (26)$$

Comparing the constraint (6) from the linear activation function case with (26), we notice that the sole distinction is that the term R_ℓ is replaced by $C_{\sigma, \ell}(R_\ell)$, which is required due to our use of the kernel trick for reducing the case of nonlinear activation functions to the linear setting.

E More Details on Matrix Approximation and Factorization Methods

As mentioned in Section 4.4, the time complexity of Algorithm 2 largely depends on the width P of each factorization matrix Q_ℓ^k and the method used to obtain it (line 3). A naive choice of $P = nm$ corresponds to solving the full kernelized problem, which can be computationally expensive. For instance, using Cholesky factorization with $P = nm$ [8] incurs a complexity of $\mathcal{O}(m^3n^3)$ and space complexity of $\mathcal{O}(m^2n^2)$.

However, to gain scalability, we use *Nystrom approximation* [48]: an approximation $\mathcal{K}_\ell^k \approx Q_\ell^k(Q_\ell^k)^\top$ for $Q_\ell^k \in \mathbb{R}^{nm \times P}$ is obtained by randomly sampling P rows/columns from the original \mathcal{K}_ℓ^k , which takes $\mathcal{O}(P^2nm)$ time. In practice, it randomly samples training examples, computes their kernel matrix and represents each training example by its similarity to the sampled examples and kernel matrix. It is well-known that this method can significantly accelerate our computations [48, 9], which is attained by using the approximate kernel matrix instead of the full one. Another advantage is that it is not necessary to compute or store the full kernel matrix, but only a submatrix requiring space complexity of $\mathcal{O}(Pmn)$.

The Nystrom method works effectively so long as the sampled training examples and the kernel matrix adequately represent the entire graph. However, if some training examples are distant from the randomly sampled ones, they may not be well-represented.

Another possible approximation method is the *random feature approximation* [35], which can be executed in $\mathcal{O}(nmP \log F_\ell)$ time [26]. Overall, using approximations significantly accelerates our algorithm's performance in terms of time and space complexity.

F Proof of Theorem 4.7

Theorem 4.7. *Consider models with a single hidden layer for binary classification (i.e., $L = G = 1$). Let $J(\cdot, \mathbf{y})$ be M -Lipchitz continuous for any fixed $\mathbf{y} \in [G]^n$ and let κ_L be either the inverse polynomial kernel or the Gaussian RBF kernel (Recall Appendices B.1-B.2). For any valid activation function σ (Recall Appendix B.3), there is a constant $C_{\sigma,L}(\mathcal{B}_L)$ such that with the radius $R_L := C_{\sigma,L}(\mathcal{B}_L)\sqrt{F}$, the expected generalization error is at most:*

$$\mathbb{E}_{\mathcal{X}, \mathbf{y}}[J(\hat{\Psi}^{\hat{A}_L}(\mathcal{X}), \mathbf{y})] \leq \inf_{\Phi \in \mathcal{F}_{gen}} \mathbb{E}_{\mathcal{X}, \mathbf{y}}[J(\Phi(\mathcal{X}), \mathbf{y})] + \frac{cMR_L \sqrt{\log(n(K+1)) \sum_{k=0}^K \mathbb{E}[\|K_L^k(\mathcal{X})\|_2]}}{\sqrt{m}} \quad (27)$$

where $c > 0$ is a universal constant.

We begin by proving several properties that apply to the general multi-class case with models comprising of multiple hidden layers, and then we specialize them to a single-hidden-layer models in the binary classification case. First, a wealthier function class shall be considered, which contains the class of GCNs. For each layer ℓ , let \mathcal{H}_ℓ be the RKHS induced by the kernel function κ_ℓ and $\|\cdot\|_{\mathcal{H}_\ell}$ be the associated Hilbert norm. Recall that, given any matrix $\mathcal{Z} \in \mathbb{R}^{(K+1) \times F_{\ell-1}}$, we denote its $(k+1)^{\text{th}}$ row as $[\mathcal{Z}]_{k+1} := \mathbf{z}_k$ for any $k \in [K] \cup \{0\}$. Using this notation, consider the following

function class:

$$\begin{aligned}
\mathcal{F}_{\text{cgcn}} &:= \{\Phi^{\mathcal{A}} = \phi^{\mathcal{A}_L} \circ \dots \circ \phi^{\mathcal{A}_1} : \phi^{\mathcal{A}_\ell} \in \mathcal{F}_{\ell, \text{cgcn}} \quad \forall \ell \in [L]\}, \text{ where} \\
\mathcal{F}_{\ell, \text{cgcn}} &:= \left\{ \phi^{\mathcal{A}_\ell} : \mathbb{R}^{n \times F_{\ell-1}^*} \rightarrow \mathbb{R}^{n \times F_\ell} : F_{\ell-1}^* < \infty \text{ and } [\phi^{\mathcal{A}_\ell}(\mathcal{X})]_{if} = \tau_\ell^f(Z_{i,\ell}(\mathcal{X})) \right. \\
&\quad \left. \text{where } \tau_\ell^f : \mathcal{Z} \in \mathbb{R}^{(K+1) \times F_{\ell-1}} \mapsto \sum_{k=0}^K \sum_{g=1}^{F_{\ell-1}^*} [\mathbf{z}_k]_g [\mathbf{a}_{\ell k}^f]_g \text{ and} \right. \\
&\quad \left. \|\tau_\ell^f\|_{\mathcal{H}_\ell} \leq C_{\sigma,\ell}(R_\ell)(K+1)\sqrt{F_\ell F_{\ell-1}} \right\} \tag{28}
\end{aligned}$$

where $C_{\sigma,\ell}(R_\ell)$ depends solely on the chosen activation function σ and the regularization parameter R_ℓ . We further consider the function class of all graph filters at layer ℓ of a standard GCN:

$$\mathcal{F}_{\ell, \text{gcn}} := \left\{ \Psi^{\mathcal{A}_\ell} : \Psi^{\mathcal{A}_\ell}(\mathcal{X}) := \sigma\left(\sum_{k=0}^K \mathcal{S}^k \mathcal{X}_{\ell-1} \mathcal{A}_{\ell k}\right) \text{ and } \max_{0 \leq k \leq K} \|\mathbf{a}_{\ell k}^f\|_2 \leq R_\ell \quad \forall f \right\} \tag{29}$$

Next, we show that the class $\mathcal{F}_{\text{cgcn}}$ contains the class of GCNs \mathcal{F}_{gcn} , making the former a richer class of functions. Particularly, the class $\mathcal{F}_{\ell, \text{cgcn}}$ of kernelized filters at layer ℓ contains the class $\mathcal{F}_{\ell, \text{gcn}}$ of all graph filters at layer ℓ corresponding to a standard GCN.

Lemma F.1. *For any valid activation function σ , there is some $C_{\sigma,\ell}(R_\ell)$ that solely depends on σ and R_ℓ such that $\mathcal{F}_{\text{gcn}} \subset \mathcal{F}_{\text{cgcn}}$. In particular, $\mathcal{F}_{\ell, \text{gcn}} \subset \mathcal{F}_{\ell, \text{cgcn}}$.*

Proof. Recall that any GCN $\Phi \in \mathcal{F}_{\text{gcn}}$ induces a nonlinear filter at each layer ℓ for the f^{th} which can be characterized by $\tau_\ell^f : \mathcal{Z} \in \mathbb{R}^{(K+1) \times F_{\ell-1}} \mapsto \sigma(\sum_{k=0}^K \langle [\mathcal{Z}]_{k+1}, \mathbf{a}_{\ell k}^f \rangle)$, i.e., the GCN Φ is given by the following composition of functions $\Phi = \tau_L \circ \dots \circ \tau_1$, where we defined $\tau_\ell : \mathbf{z} \mapsto (\tau_\ell^f(\mathbf{z}))_{f \in [F_\ell]}$. Given any valid activation function, Corollary B.1 and Corollary B.3 yield that τ_ℓ^f resides within the reproducing kernel Hilbert space \mathcal{H}_ℓ and its Hilbert norm is upper bounded as $\|\tau_\ell^f\|_{\mathcal{H}_\ell} \leq C_\sigma(\|\sum_{k=0}^K \mathbf{a}_{\ell k}^f\|_2) \leq C_\sigma(R_\ell)\sqrt{K+1}$, which clearly satisfies the constraint in (28) for any layer ℓ , as desired. \square

Recalling that $\hat{\Psi}^{\hat{\mathcal{A}}_\ell}(\cdot)$ is the predictor at each layer ℓ produced by Algorithm 2, we now formally prove that the predictor $\hat{\Psi}^{\hat{\mathcal{A}}_L}(\cdot)$ generated at the last layer is an empirical risk minimizer in the function class $\mathcal{F}_{\text{cgcn}}$.

Lemma F.2. *By running Algorithm 2 with the regularization parameter $\mathcal{B}_\ell = C_{\sigma,\ell}(R_\ell)\sqrt{F_\ell F_{\ell-1}}$ at layer ℓ , the predictor $\hat{\Psi}^{\hat{\mathcal{A}}_L}(\cdot)$ generated at the last layer satisfies:*

$$\hat{\Psi}^{\hat{\mathcal{A}}_L} \in \arg \min_{\Phi \in \mathcal{F}_{\text{cgcn}}} \frac{1}{m} \sum_{j=1}^m J(\Phi(\mathcal{X}^{(j)}), y^{(j)}) \tag{30}$$

Proof. Consider the function class of all CGCNs whose filters at layer ℓ have a nuclear norm of at

most \mathcal{B}_ℓ , given by:

$$\mathcal{F}_{\mathcal{B}_\ell} := \left\{ \Phi^{\mathcal{A}} = \Psi^{\mathcal{A}_L} \circ \dots \circ \Psi^{\mathcal{A}_1} \left| \Psi^{\mathcal{A}_\ell} : \mathcal{X} \mapsto \sum_{k=0}^K \mathcal{S}^k \mathcal{X}_{\ell-1} \mathcal{A}_{\ell k} \text{ and } \right. \right. \\ \left. \left. \mathcal{A}_{\ell k} \in \mathbb{R}^{F_{\ell-1} \times F_\ell} \text{ and } \|\mathcal{A}_\ell\|_* \leq \mathcal{B}_\ell \right\} \quad (31)$$

Our goal is thus proving that $\mathcal{F}_{\mathcal{B}_\ell} \subset \mathcal{F}_{\text{cgcn}}$, and that any empirical risk minimizer in $\mathcal{F}_{\text{cgcn}}$ is also in $\mathcal{F}_{\mathcal{B}_\ell}$. We begin with showing that $\mathcal{F}_{\mathcal{B}_\ell} \subset \mathcal{F}_{\text{cgcn}}$. Let $\Phi^{\mathcal{A}} = \Psi^{\mathcal{A}_L} \circ \dots \circ \Psi^{\mathcal{A}_1} \in \mathcal{F}_{\mathcal{B}_\ell}$ such that $\Psi^{\mathcal{A}_\ell}(\mathcal{X}) = \sum_{k=0}^K \mathcal{S}^k \mathcal{X}_{\ell-1} \mathcal{A}_{\ell k}$ with $\|\mathcal{A}_\ell\|_* \leq \mathcal{B}_\ell$ for any $\ell \in [L]$. We shall prove that $\Psi^{\mathcal{A}_\ell} \in \mathcal{F}_{\ell, \text{cgcn}}$. Indeed, consider the singular value decomposition (SVD) of $\mathcal{A}_{\ell k}$, which we assume is given by $\mathcal{A}_{\ell k} = \sum_{s \in [F_{\ell-1}^*]} \lambda_{\ell ks} \mathbf{w}_{\ell ks} \mathbf{u}_{\ell ks}^\top$ for some $F_{\ell-1}^* < \infty$, where each left-singular vector $\mathbf{w}_{\ell ks}$ and each right-singular vector $\mathbf{u}_{\ell ks}$ are both unit column vectors, while each singular value $\lambda_{\ell ks}$ is a real number. Therefore, the filters corresponding to the f^{th} feature can be written as:

$$\mathbf{a}_{\ell k}^f = \sum_{s \in [F_{\ell-1}^*]} \lambda_{\ell ks} [\mathbf{w}_{\ell ks}]_f \cdot \mathbf{u}_{\ell ks}^\top = \sum_{s \in [F_{\ell-1}^*]} \lambda_{\ell ks} w_{\ell ks}^f \cdot \mathbf{u}_{\ell ks}^\top \quad (32)$$

As such, the value of the f^{th} feature of node i under $\Psi^{\mathcal{A}_\ell}$ can be rephrased as:

$$[\Psi^{\mathcal{A}_\ell}(\mathcal{X})]_{if} = \sum_{k=0}^K \sum_{g=1}^{F_{\ell-1}} [\mathbf{z}_i^k(\mathcal{X}_{\ell-1})]_g [\mathbf{a}_{\ell k}^f]_g = \sum_{k=0}^K \left\langle \mathbf{z}_i^k(\mathcal{X}_{\ell-1}), \sum_{s \in [F_{\ell-1}^*]} \lambda_{\ell ks} w_{\ell ks}^f \mathbf{u}_{\ell ks}^\top \right\rangle \quad (33)$$

Let $\mathbf{v}_\ell^k(\mathbf{z}) \in \mathbb{R}^{nm}$ be a vector whose (i, j) -th coordinate equals to $\kappa_\ell(\mathbf{z}, \mathbf{z}_i^k(\mathcal{X}_{\ell-1}^{(j)}))$. Similarly to Appendix D, denote $\tau_\ell^f(\mathbf{z}) := \sum_{k=0}^K \langle (Q_\ell^k)^\dagger \mathbf{v}_\ell^k(\mathbf{z}), \sum_{s \in [F_{\ell-1}^*]} \lambda_{\ell ks} w_{\ell ks}^f \mathbf{u}_{\ell ks}^\top \rangle$. For any matrix $\mathcal{Z} \in \mathbb{R}^{(K+1) \times F_{\ell-1}}$ whose $(k+1)^{\text{th}}$ row is given by $[\mathcal{Z}]_{k+1} := \mathbf{z}_k$ for any $k \in [K] \cup \{0\}$, note that τ_ℓ^f can be rephrased as $\tau_\ell^f(\mathbf{z}) := \sum_{k=0}^K \langle \mathbf{v}_\ell^k(\mathbf{z}), ((Q_\ell^k)^\top)^\dagger \sum_{s \in [F_{\ell-1}^*]} \lambda_{\ell ks} w_{\ell ks}^f \mathbf{u}_{\ell ks}^\top \rangle$. Thus, (22) implies that the Hilbert norm of the function τ_ℓ^f satisfies:

$$\begin{aligned} \|\tau_\ell^f\|_{\mathcal{H}_\ell} &\leq \sum_{k=0}^K \left\| (Q_\ell^k)^\top ((Q_\ell^k)^\top)^\dagger \sum_{s \in [F_{\ell-1}^*]} \lambda_{\ell ks} w_{\ell ks}^f \mathbf{u}_{\ell ks}^\top \right\|_2 \leq \sum_{k=0}^K \left\| \sum_{s \in [F_{\ell-1}^*]} \lambda_{\ell ks} w_{\ell ks}^f \mathbf{u}_{\ell ks}^\top \right\|_2 \\ &\leq \sum_{k=0}^K \sum_{s \in [F_{\ell-1}^*]} |\lambda_{\ell ks}| \cdot |w_{\ell ks}^f| \cdot \|\mathbf{u}_{\ell ks}^\top\|_2 \\ &\leq \sum_{k=0}^K \sum_{s \in [F_{\ell-1}^*]} |\lambda_{\ell ks}| = \sum_{k=0}^K \|\mathcal{A}_{\ell k}\|_* \leq C_{\sigma, \ell}(R_\ell)(K+1)\sqrt{F_\ell F_{\ell-1}} \end{aligned} \quad (34)$$

where we used the triangle inequality and the fact that the singular vectors are unit vectors. Since $[\Psi^{\mathcal{A}_\ell}(\mathcal{X})]_{if} = \tau_\ell^f(\mathcal{Z}_{i, \ell}(\mathcal{X}_{\ell-1}))$, we obtained that $\mathcal{F}_{\mathcal{B}_\ell} \subset \mathcal{F}_{\text{cgcn}}$, as desired.

To conclude the proof, we next prove that any empirical risk minimizer $\Phi^{\mathcal{A}}$ in $\mathcal{F}_{\text{cgcn}}$ is also in $\mathcal{F}_{\mathcal{B}_\ell}$. By our proof in Appendix D, the value of the f^{th} feature of node i at layer ℓ is then

given by $\tau_\ell^f(\mathcal{Z}_{i,\ell}(\mathcal{X}_{\ell-1}^{(j)}))$, where, as specified in (25), $\tau_\ell^f(\mathcal{Z}) = \sum_{k=0}^K \langle (Q_\ell^k)^\dagger \mathbf{v}_\ell^k(\mathbf{z}_k), (Q_\ell^k)^\top \beta_{\ell k}^f \rangle$ is a reparameterization of the graph filters at layer ℓ for some vector of the coefficients $\beta_{\ell k}^f \in \mathbb{R}^{nm}$ whose (i, j) -th coordinate is $\beta_{\ell k, (i, j)}^f$. That is, $(Q_\ell^k)^\top \beta_{\ell k}^f$ now act as the filters under this reparameterization. In Appendix D, we have shown that the Hilbert norm of τ_ℓ^f is then $\|\tau_\ell^f\|_{\mathcal{H}_\ell} = \|(Q_\ell^k)^\top \beta_{\ell k}^f\|_2 \leq C_{\sigma, \ell}(R_\ell)$, where the last inequality is by (22). By (26), we further infer that the nuclear norm of the filters $(Q_\ell^k)^\top \beta_{\ell k}^f$ in the new parameterization satisfies $\|(Q_\ell^k)^\top \beta_{\ell k}^f\|_* \leq C_{\sigma, \ell}(R_\ell) \sqrt{F_\ell F_{\ell-1}(K+1)} \leq C_{\sigma, \ell}(R_\ell)(K+1) \sqrt{F_\ell F_{\ell-1}}$, meaning that $\Phi^A \in \mathcal{F}_{\mathcal{B}_\ell}$, as desired. \square

Next, we prove that $\mathcal{F}_{L, \text{cgc}}n$ is not "too big" by upper bounding its Rademacher complexity. The Rademacher complexity is a key concept in empirical process theory and can be used to bound the generalization error in our empirical risk minimization problem. Readers should refer to [2] for a brief overview on Rademacher complexity. The *Rademacher complexity* of a function class $\mathcal{F} = \{\phi : \mathcal{D} \rightarrow \mathbb{R}\}$ with respect to m i.i.d samples $\{\mathcal{X}^{(j)}\}_{j=1}^m$ is given by:

$$\mathcal{R}_m(\mathcal{F}) := \mathbb{E}_{\mathcal{X}, \varepsilon} \left[\sup_{\phi \in \mathcal{F}} \frac{1}{m} \sum_{j=1}^m \varepsilon_j \phi(\mathcal{X}^{(j)}) \right] \quad (35)$$

where $\{\varepsilon_j\}_{j=1}^m$ are an i.i.d. sequence of uniform $\{\pm 1\}$ -valued variables. Next, we provide the upper bound on the Rademacher complexity of the function class $\mathcal{F}_{L, \text{cgc}}n$ describing the graph filters. The lemma refers to the random kernel matrix $\mathcal{K}_\ell^k(\mathcal{X}) \in \mathbb{R}^{n \times n}$ induced by a graph signal $\mathcal{X} \in \mathbb{R}^{n \times F}$ drawn randomly from the population, i.e., the (i, i') -th entry of $\mathcal{K}_\ell^k(\mathcal{X})$ is $\kappa_\ell(\mathbf{z}_i^k(\mathcal{X}), \mathbf{z}_{i'}^k(\mathcal{X}))$. Furthermore, we consider the expectation $\mathbb{E}[\|\mathcal{K}_\ell^k(\mathcal{X})\|_2]$ of this matrix's spectral norm. While the previous lemmas consider the most general case where the number of features $F_L = G$ at the last layer may be any positive integer, observe that the following result focuses on the the binary classification case where $F_L = G = 1$. As mentioned in Section 4.5, Lemma F.3 can be readily extended to the multi-class case by employing a standard one-versus-all reduction to the binary case.

Lemma F.3. *In the binary classification case where $F_L = G = 1$, there exists a universal constant $c > 0$ such that:*

$$\mathcal{R}_m(\mathcal{F}_{L, \text{cgc}}n) \leq \frac{c \cdot C_{\sigma, \ell}(\mathcal{B}_L) \sqrt{F_{\ell-1}(K+1) \cdot \log(n(K+1)) \cdot \sum_{k=0}^K \mathbb{E}[\|\mathcal{K}_L^k(\mathcal{X})\|_2]}{\sqrt{m}} \quad (36)$$

Proof. We begin with some preliminaries that apply to the general case and then leverage them in order to obtain the result. For brevity, we denote $R_\ell = C_{\sigma, \ell}(\mathcal{B}_\ell) \sqrt{F_\ell F_{\ell-1}}$. Consider some function $\Phi^A = \phi^{A_L} \circ \dots \circ \phi^{A_1} \in \mathcal{F}_{\text{cgc}}n$. Without loss of generality, we assume that, each input graph signal $\mathcal{X}^{(j)}$, the feature vector $[\mathcal{X}^{(j)}]_i = \mathbf{x}_i^{(j)}$ of each node i resides in the unit ℓ_2 -ball (which can be obtain via normalization). Combined with κ_ℓ 's being a continuous kernel with $\kappa_\ell(\mathbf{z}, \mathbf{z}) \leq 1$, Mercer's theorem [44, Theorem 4.49] implies that there exists a feature map $\varphi_\ell : \mathbb{R}^{F_{\ell-1}} \rightarrow \ell^2(\mathbb{N})$ for which $\sum_{\xi=1}^\infty [\varphi_\ell(\mathbf{z})]_\xi [\varphi_\ell(\mathbf{z}')]_\xi = \sum_{\xi=1}^\infty \varphi_{\ell\xi}(\mathbf{z}) \varphi_{\ell\xi}(\mathbf{z}')$ converges uniformly and absolutely to $\kappa_\ell(\mathbf{z}, \mathbf{z}')$. Accordingly, it holds that $\kappa_\ell(\mathbf{z}, \mathbf{z}') = \langle \varphi_\ell(\mathbf{z}), \varphi_\ell(\mathbf{z}') \rangle$, which yields the following for each feature f of any node i at layer ℓ is $\tau_\ell^f(\mathcal{Z}_{i,\ell}(\mathcal{X}_{\ell-1}))$, where for any matrix $\mathcal{Z} \in \mathbb{R}^{(K+1) \times F_{\ell-1}}$ whose $(k+1)^{\text{th}}$ row is given by $[\mathcal{Z}]_{k+1} := \mathbf{z}_k$ for any $k \in [K] \cup \{0\}$:

$$\tau_\ell^f(\mathcal{Z}) := \sum_{k=0}^K \langle \varphi_\ell(\mathbf{z}_k), \bar{\mathbf{a}}_{\ell k}^f \rangle \quad (37)$$

where $\bar{\mathbf{a}}_{\ell k}^f \in \ell^2(\mathbb{N})$ is a countable-dimensional vector, due to the fact that φ itself is a countable sequence of functions. Particularly, the Hilbert norm of τ_ℓ^f is $\|\tau_\ell^f\|_{\mathcal{H}_\ell} = \|\bar{\mathbf{a}}_{\ell k}^f\|_2$. Now, for any graph signal \mathcal{X} , let $\Theta_i(\mathcal{X})$ be the linear operator that maps any sequence $\theta \in \ell^2(\mathbb{N})$ to the vector $[\langle \varphi_\ell(\mathbf{z}_i^0(\mathcal{X})), \theta \rangle, \dots, \langle \varphi_\ell(\mathbf{z}_i^K(\mathcal{X})), \theta \rangle]^\top \in \mathbb{R}^{K+1}$. Thereby, recalling that $\Phi^{\mathcal{A}} = \phi^{\mathcal{A}_L} \circ \dots \circ \phi^{\mathcal{A}_1}$ where $\phi^{\mathcal{A}_\ell} \in \mathcal{F}_{\ell, cgc n}$ satisfies $[\phi^{\mathcal{A}_\ell}(\mathcal{X}_{\ell-1})]_{if} = \tau_\ell^f(\mathcal{Z}_{i,\ell}(\mathcal{X}_{\ell-1}))$, then the f^{th} feature of node i at layer ℓ can be rephrased as:

$$\begin{aligned} [\phi^{\mathcal{A}_\ell}(\mathcal{X}_{\ell-1})]_{if} &= \mathbf{1}_{K+1}^\top \Theta_i(\mathcal{X}_{\ell-1}) \bar{\mathbf{a}}_{\ell k}^f = \text{trace} \left(\Theta_i(\mathcal{X}_{\ell-1}) (\bar{\mathbf{a}}_{\ell k}^f \mathbf{1}_{K+1}^\top) \right) \\ \Rightarrow \phi^{\mathcal{A}_\ell}(\mathcal{X}_{\ell-1}) &= \left[\text{trace} \left(\Theta_i(\mathcal{X}_{\ell-1}) (\bar{\mathbf{a}}_{\ell k}^f \mathbf{1}_{K+1}^\top) \right) \right]_{i \in [n], f \in [F_\ell]} \end{aligned} \quad (38)$$

where $\mathbf{1}_{K+1}$ is the all-ones vector of dimension $K+1$. Note that the matrix $\bar{\mathcal{A}}_{\ell k} := \bar{\mathbf{a}}_{\ell k}^f \mathbf{1}_{K+1}^\top$ satisfies the following:

$$\|\bar{\mathcal{A}}_{\ell k}\|_* = \|\bar{\mathbf{a}}_{\ell k}^f \mathbf{1}_{K+1}^\top\|_* \leq \|\mathbf{1}_{K+1}^\top\|_2 \cdot \|\bar{\mathbf{a}}_{\ell k}^f\|_2 = \|\tau_\ell^f\|_{\mathcal{H}_\ell} \sqrt{K+1} \leq R_\ell \sqrt{K+1} \quad (39)$$

Now, we obtain our upper bound for the binary classification case where $F_L = G = 1$. Combining (38) with (39), we obtain that the Rademacher complexity of $\mathcal{F}_{L, cgc n}$ is upper bounded as follows:

$$\begin{aligned} \mathcal{R}_m(\mathcal{F}_{L, cgc n}) &= \mathbb{E} \left[\sup_{\phi^{\mathcal{A}_L} \in \mathcal{F}_{L, cgc n}} \frac{1}{m} \sum_{j=1}^m \varepsilon_j \Phi^{\mathcal{A}_L}(\mathcal{X}^{(j)}) \right] = \\ &= \frac{1}{m} \mathbb{E} \left[\sup_{\|\bar{\mathcal{A}}_{Lk}\|_* \leq R_L \sqrt{K+1}} \text{trace} \left(\left(\sum_{j=1}^m \varepsilon_j \Theta_i(\mathcal{X}_{L-1}^{(j)}) \right) \bar{\mathcal{A}}_{Lk} \right) \right] \\ &\leq \frac{R_L \sqrt{K+1}}{m} \mathbb{E} \left[\left\| \sum_{j=1}^m \varepsilon_j \Theta_i(\mathcal{X}_{L-1}^{(j)}) \right\|_2 \right] \end{aligned} \quad (40)$$

where the last equality uses Hölder's inequality while using the duality between the nuclear norm and the spectral norm. Next, note that $\sum_{j=1}^m \varepsilon_j \Theta_i(\mathcal{X}_{L-1}^{(j)})$ can be thought of as a matrix with n rows and infinitely many columns. We denote its sub-matrix comprising of the first r columns as $\Theta_i^{(r)}(\mathcal{X}_{L-1}^{(j)})$ and let $\Theta_i^{(-r)}(\mathcal{X}_{L-1}^{(j)})$ be the remaining sub-matrix. Therefore:

$$\mathbb{E} \left[\left\| \sum_{j=1}^m \varepsilon_j \Theta_i(\mathcal{X}_{L-1}^{(j)}) \right\|_2 \right] \quad (41a)$$

$$\leq \mathbb{E} \left[\left\| \sum_{j=1}^m \varepsilon_j \Theta_i^{(r)}(\mathcal{X}_{L-1}^{(j)}) \right\|_2 \right] + \left(\mathbb{E} \left[\left\| \sum_{j=1}^m \varepsilon_j \Theta_i^{(-r)}(\mathcal{X}_{L-1}^{(j)}) \right\|_F^2 \right] \right)^{1/2} \quad (41b)$$

$$\leq \mathbb{E} \left[\left\| \sum_{j=1}^m \varepsilon_j \Theta_i^{(r)}(\mathcal{X}_{L-1}^{(j)}) \right\|_2 \right] + \left(nm \mathbb{E} \left[\sum_{\xi=r+1}^\infty (\varphi_{\ell \xi}(\mathbf{z}))^2 \right] \right)^{1/2} \quad (41c)$$

Since $\sum_{\xi=1}^\infty (\varphi_{\ell \xi}(\mathbf{z}))^2$ uniformly converges to $\kappa_\ell(\mathbf{z})$, the second term in (41c) converges to 0 as $r \rightarrow \infty$. Hence, it is sufficient to upper bound the first term in (41c) and take the limit $r \rightarrow \infty$. By

Bernstein inequality due to [30, Theorem 2.1], whenever $\text{trace}(\Theta_i^{(r)}(\mathcal{X}_{L-1}^{(j)})\Theta_i^{(r)}(\mathcal{X}_{L-1}^{(j)})^\top) \leq C_1$, there is a universal constant $c > 0$ such that the expected spectral norm is upper bounded by:

$$\begin{aligned} \mathbb{E} \left[\left\| \sum_{j=1}^m \varepsilon_j \Theta_i^{(r)}(\mathcal{X}_{L-1}^{(j)}) \right\|_2 \right] &\leq c \sqrt{\log(mC_1)} \mathbb{E} \left[\left(\sum_{j=1}^m \left\| \Theta_i^{(r)}(\mathcal{X}_{L-1}^{(j)}) \Theta_i^{(r)}(\mathcal{X}_{L-1}^{(j)})^\top \right\|_2 \right)^{1/2} \right] \\ &\leq c \sqrt{\log(mC_1)} (m \mathbb{E}[\|\Theta_i(\mathcal{X})\Theta_i(\mathcal{X})^\top\|_2])^{1/2} \quad (42) \\ &\leq c \sqrt{\log(mC_1)} \left(m \sum_{k=0}^K \mathbb{E}[\|K_L^k(\mathcal{X})\|_2] \right)^{1/2} \end{aligned}$$

Notice that, due to the uniform kernel expansion $\kappa_\ell(\mathbf{z}, \mathbf{z}') = \sum_{\xi=1}^\infty \varphi_{\ell\xi}(\mathbf{z})\varphi_{\ell\xi}(\mathbf{z}')$, it holds that the trace norm is bounded as $\text{trace}(\Theta_i^{(r)}(\mathcal{X}_{L-1}^{(j)})\Theta_i^{(r)}(\mathcal{X}_{L-1}^{(j)})^\top) \leq K+1$ since $\kappa_\ell(\mathbf{z}, \mathbf{z}') \leq 1$. Combining this with (42) and (40) implies the desired in (36). \square

We are ready to prove the key lemma that will yield our main result. Recall that our current focus is on binary classification (i.e., $F_L = G = 1$). While our prior results consider models with multiple hidden layers, our main result regards the case of a single hidden layer $L = 1$. As mentioned in Section 4.5, in the case of multiple hidden layers, our result applies to each individual layer separately. Using Lemmas F.1–F.3, we are capable of comparing the CGCN predictor obtained by Algorithm 2 against optimal model in the GCN class. Lemma F.2 yields that the predictor $\hat{\Psi}^{\hat{\mathcal{A}}_L}(\cdot)$ generated at the last layer is an empirical risk minimizer in the function class $\mathcal{F}_{\text{cgcn}}$. As such, by the theory of Rademacher complexity (see, e.g., [2]), we obtain that:

$$\mathbb{E}_{\mathcal{X}, \mathbf{y}}[J(\hat{\Psi}^{\hat{\mathcal{A}}_L}(\mathcal{X}), \mathbf{y})] \leq \inf_{\Phi \in \mathcal{F}_{L, \text{cgcn}}} \mathbb{E}_{\mathcal{X}, \mathbf{y}}[J(\Phi(\mathcal{X}), \mathbf{y})] + 2M \cdot \mathcal{R}_m(\mathcal{F}_{L, \text{cgcn}}) + \frac{c}{\sqrt{m}} \quad (43)$$

where c is a universal constant and we used the assumption that J is M -Lipschitz. By Lemma F.1, we have that $\inf_{\Phi \in \mathcal{F}_{L, \text{cgcn}}} \mathbb{E}_{\mathcal{X}, \mathbf{y}}[J(\Phi(\mathcal{X}), \mathbf{y})] \leq \inf_{\Phi \in \mathcal{F}_{L, \text{gcn}}} \mathbb{E}_{\mathcal{X}, \mathbf{y}}[J(\Phi(\mathcal{X}), \mathbf{y})]$. Since $\mathcal{F}_{\text{cgcn}} = \mathcal{F}_{1, \text{cgcn}}$ due to $L = 1$, this means that $\inf_{\Phi \in \mathcal{F}_{\text{cgcn}}} \mathbb{E}_{\mathcal{X}, \mathbf{y}}[J(\Phi(\mathcal{X}), \mathbf{y})] \leq \inf_{\Phi \in \mathcal{F}_{\text{gcn}}} \mathbb{E}_{\mathcal{X}, \mathbf{y}}[J(\Phi(\mathcal{X}), \mathbf{y})]$. Combined with (43), we obtain the desired.

Remark F.4. The constant $C_{\sigma, L}(\mathcal{B}_L)$ depends on the convergence rate of the polynomial expansion of the activation function σ (See Appendix B). Algorithmically, knowing the activation function is not required to run Algorithm 2. Theoretically, however, the choice of σ matters for Theorem 4.7 when comparing the predictor produced by Algorithm 2 against the best GCN, as it affects the representation power of such GCN. If a GCN with an activation function σ performs well, CGCN will similarly generalize strongly.

G Additional Experimental Details

G.1 Dataset Descriptions

Table 2 provides a summary of the statistics and characteristics of datasets used in this paper. All datasets are accessed using the TUDataset class [31] in PyTorch Geometric [14] (MIT License).

Table 2: Statistics of the graph classification datasets used in our experiments.

Dataset	#Graphs	Avg. Nodes	Avg. Edges	#Classes
MUTAG	118	18	20	2
PTC-MR	344	26	51	2
PROTEINS	1,113	39	73	2
NCI1	4,110	30	32	2
Mutagenicity	4,337	30	31	2

G.2 Additional Implementation Details

Hardware and Software. All experiments could fit on one GPU at a time. Most experiments were run on a server with 4 NVIDIA L40S GPUs. We ran all of our experiments in Python, using the PyTorch framework [34] (license URL). We also make use of PyTorch Geometric (PyG) [14] (MIT License) for experiments with graph data.

Implementation Details. Particularly, all models were implemented using PyTorch Geometric (PyG) [14]. For GATv2 and GraphGPS, we use the official PyG implementations of their original papers, while for other baselines we use their PyG implementations, as standard in prior works (see, e.g., [32, 36]). Each neural architecture consists of $L \in \{2, 6\}$ layers of the considered baseline, followed by a Set2Set global pooling [46] to aggregate the learned node-level representations to a graph-level embedding and a two-layer MLP for the final classification. The embedding dimension of each hidden layer is set to 64, while non-convex models use a ReLU activation function between layers. For convex models, we use the Gaussian RBF kernel $\kappa(\mathbf{z}, \mathbf{z}') := \exp(-\gamma \|\mathbf{z} - \mathbf{z}'\|_2^2)$ with $\gamma = 0.2$, and compute an approximate kernel matrix via Nyström approximation [48] with dimension $P = 64$ (Recall Section 4.4). As we want to evaluate the performance of GNN models in isolation, note that we do not use DropOut or batch normalization. Further, since we do not focus on the impact of attention heads on performance, all convex and non-convex versions of GAT, GATv2, GraphTrans and GraphGPS use their default configurations of attention heads.

H Additional Experimental Results

H.1 Heatmap of Classification Accuracy

Figure 2 provides a heatmap summarizing the accuracy of all models across the different datasets. It complements Table 1 by visually reinforcing that convex models generally outperform their non-convex counterparts across nearly all datasets, with consistent and major improvements even for models like GATv2 and GraphGPS. This reaffirms the strength and generality of our convexification framework. For example, on MUTAG, the convex CGIN model reaches 83.2% accuracy, outperforming the two-layer (60.0%) and six-layer (61.2%) GINs. Similarly, CGraphGPS achieves 83.7%, exceeding the best non-convex variant by over 30%. This trend holds across other datasets like PTC-MR, PROTEINS, and NCI1, where convex versions of CGraphSAGE, CGATv2, and CGraphGPS outperform non-convex baselines by 10–40%.

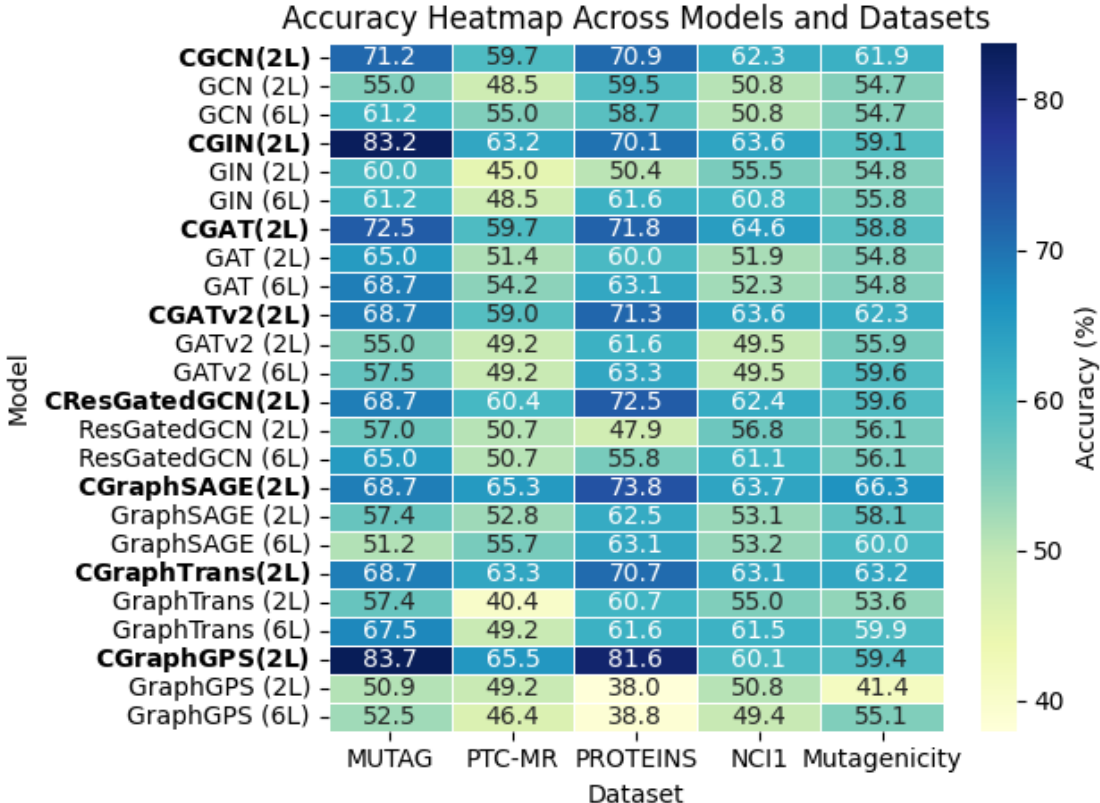


Figure 2: Heatmap of classification accuracy (%) across all models and datasets. Rows correspond to models, columns to datasets. The names of convex models are **bolded** to emphasize their performance.

H.2 Bar Plots

The bar plots in Figure 3 highlight the consistent performance advantage of convex models over their non-convex counterparts across multiple datasets in a more straightforward way than numerical data alone. They further underscore how convex architectures provide not just dataset-specific improvements, but a general trend of robustness and high accuracy, even in the absence of large training sets. This emphasizes that our convex models harness stable optimization landscapes, enabling reliable learning where non-convex models exhibit erratic performance due to training instabilities.

H.3 Radar Plots

The radar plots in Figure 4 offer a holistic view of how convex models perform across diverse datasets. They reveal that convex variants not only perform strongly on small datasets like MUTAG and PTC-MR, but also remain competitive or superior on larger datasets such as NCI1 and Mutagenicity. This multi-dimensional consistency further challenges the notion that expressive representations require deep, non-convex architectures, and instead supports that convex shallow models, when carefully designed, can adapt well across a spectrum of tasks and data scales.

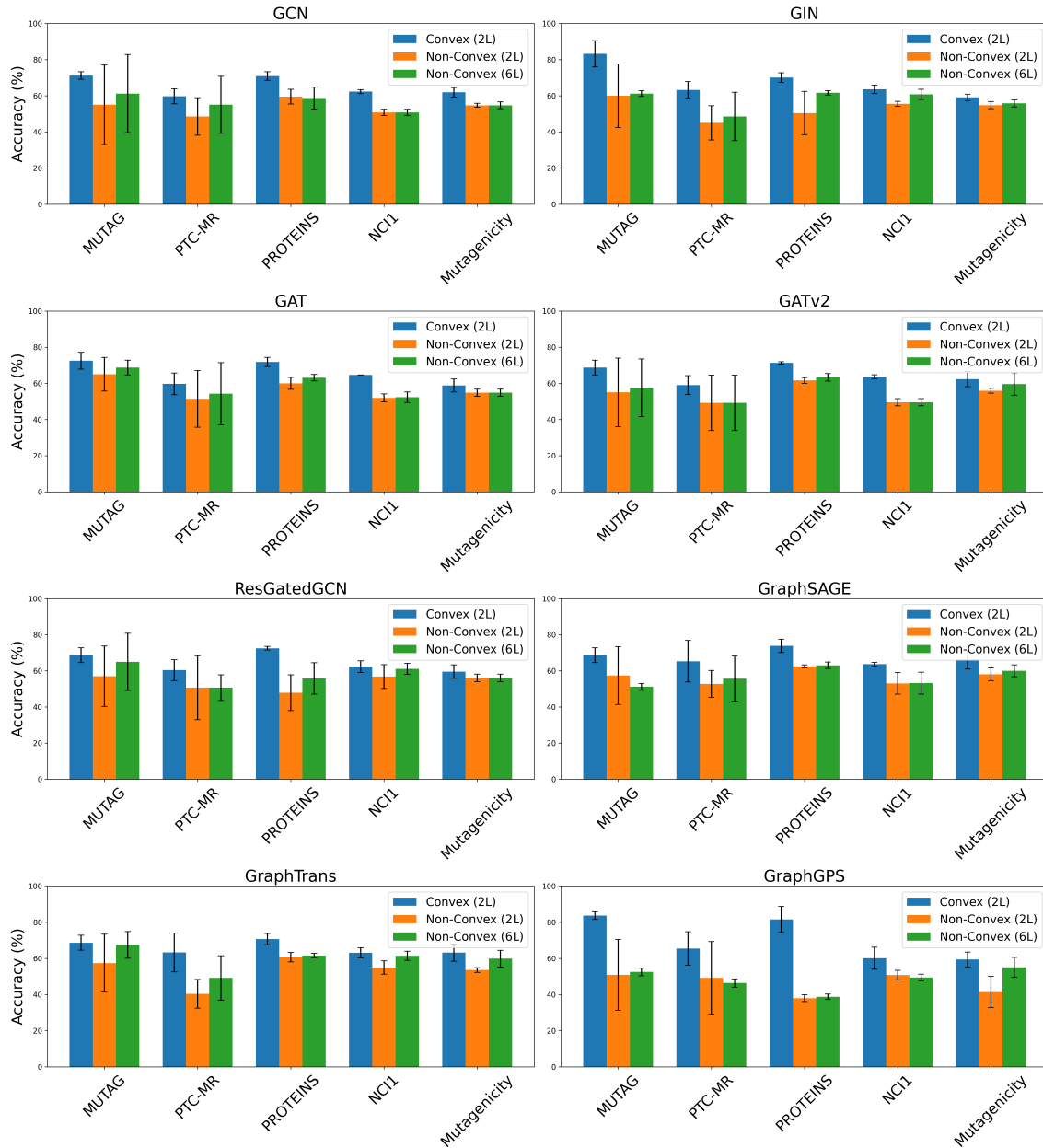


Figure 3: Accuracy comparison of two-layer convex GNNs (prefixed with ‘C’) against their standard two-layer and six-layer non-convex counterparts across five graph classification datasets. Bars represent the mean accuracy over four runs, and error bars denote the standard deviation. Datasets are ordered from left to right by increasing size.

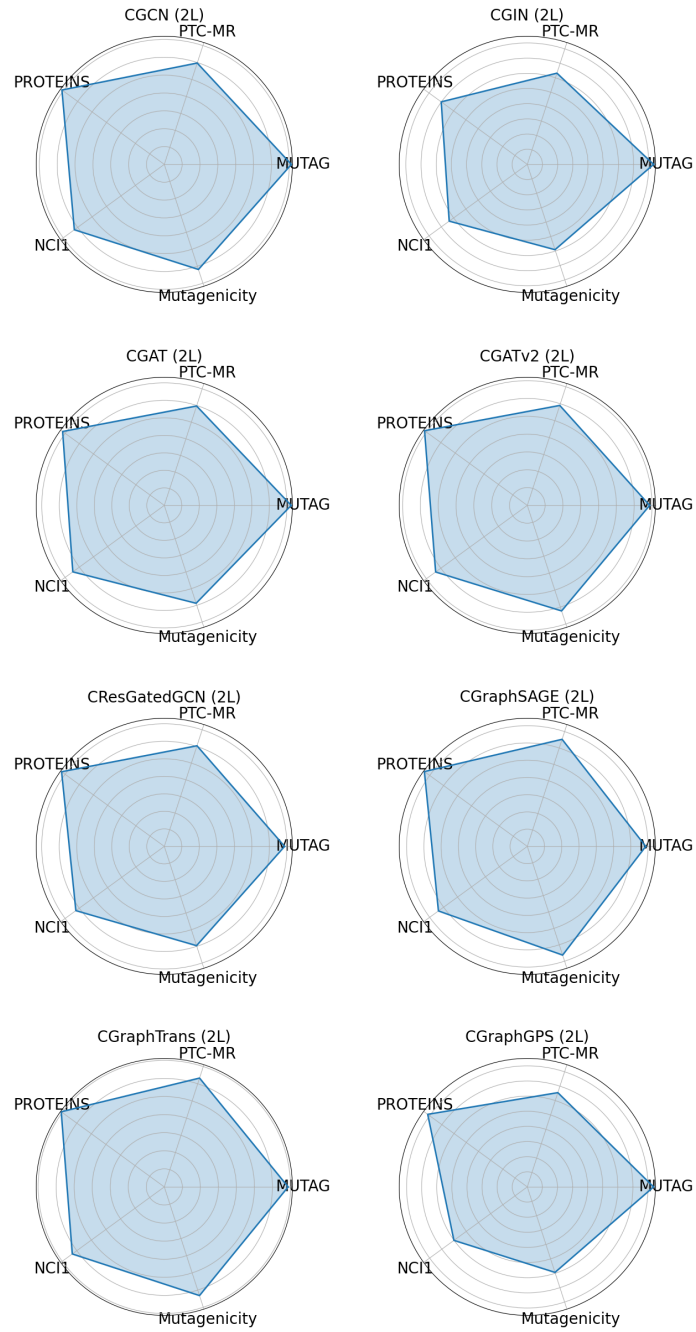


Figure 4: Radar plots showing the performance of each two-layer convex model across five graph classification datasets. Each axis corresponds to a dataset, with higher values indicating better classification accuracy. These plots illustrate the consistency and robustness of convex models across diverse graph types.